Mineralisation controls for the diverse Cape manganese occurrences, South Africa

B.P. von der Heyden, R.A. La Cock and D.R. Ferreira
Department of Earth Sciences, Stellenbosch University, Private Bag X1, Matieland 7602, South Africa
e-mail: bvon@sun.ac.za; 0000-0002-4006-9278; lacockrutger@gmail.com; 21656118@sun.ac.za

T.A. Conradie
Department of Microbiology, Stellenbosch University, Private Bag X1, Matieland 7602, South Africa
e-mail: tcon@sun.ac.za

J.D. van Rooyen
Department of Earth Sciences, Stellenbosch University, Private Bag X1, Matieland 7602, South Africa
e-mails: jvan@sun.ac.za

L. Palcsu
Isotope Climatology and Environmental Research Centre (ICER), Institute for Nuclear Research, H-4026, Debrecen, Bem tér 18/c, Hungary
e-mail: palcsu.laszlo@atomki.mta.hu

Abstract

The Cape Fold Belt, comprising folded sedimentary sequences from predominantly the Palaeozoic Cape Supergroup, hosts a multitude of manganese occurrences and mineral deposits, many of which were subject to historical mining activity. Although size, grade and quality issues negate their modern-day exploitation for the steel-making process, the mechanisms by which Mn has enriched at these sites holds scientific value for our understanding of low-temperature Mn (bio-)geochemical cycling. Deposits located within the Cape Fold Belt comprise structure-hosted Mn deposits and a little described class of Mn mound deposits associated with chalybeate thermal springs (temperature = 41 to 48°C). Although the relationships between the two remain tenuous, detailed study of both classes provides insight into the conditions that favour Mn accumulation in the near-surface and sub-aerial environments. Comparisons between the physicochemistry of manganiferous- and non-manganiferous thermal springs suggest that manganese solubility is favoured by warm, acidic and slightly reducing fluids with elevated salinity. Transport, and associated fluid focusing typically within highly permeable sandstone units, serves to locate Mn mineralisation in near-surface structurally-complex trap sites that provide both accommodation space and conditions that are sufficiently oxidising. Where manganiferous spring waters spill out at surface, oxidation is caused by contact with atmospheric O_2 to form Mn mound deposits, and ambient Mn-oxidising microbiota (e.g., genus Ramlibacter, and members of Burkholderiales, Rhodocyclaceae, and Oxalobacteraceae) are likely to play a role in enhancing the kinetics of this process. Relative to the structure-hosted deposits, these Mn mound deposits are typically lower grade (higher iron content) and relatively friable (high porosity and fine grain sizes). Supergene and diagenetic processes can lead to localised upgrade of the Mn mound material, although typically not to ore grade.

Introduction

Manganese occurrences within the *ca*. 510 to 350 Ma Cape Supergroup, which exist predominantly as structurally-controlled veins or localised breccia zones in competent sandstone units, were first identified in the late nineteenth century (Welsh, 1917; de Villiers, 1960; Jones, 2010). Because South Africa has vast reserves of this commodity in especially the Kalahari Manganese Field (e.g., Beukes et al., 2016) and because the majority of the eighteen historically-mined Mn occurrences (Cole et al., 2014) within the Cape Supergroup have been mined out or were deemed sub-economic, many of the Cape Mn deposits have received little scientific or industrial attention. However, with modern uses of Mn expanding well beyond its primary use in steel-making to incorporate industries such as the battery sector, the chemicals sector (bleaching agent, redox active properties, catalyst), and the fertilizer sector (Steenkamp et al., 2020; USGS, 2023), Mn deposits and the science underpinning Mn biogeochemical cycling are receiving renewed interest across the globe.

Manganese occurrences in brittle and fractured sandstone units have been documented globally. For example, a number of small near-surface 'fissure' vein deposits have been mined in southeastern Utah, USA where they form preferentially in permeable sandstone units (Baker et al., 1952), likely through the involvement of reducing, saline brine (Chan et al., 2000). Similarly, Carmichael and coworkers (2017) noted a spatial relationship between mapped regional faults, associated deformation, and vein-hosted and breccia-cement Mn occurrences in Tennessee and Virginia (USA). In Scotland, detailed geochemical work revealed that Mn^{4+}-rich vein deposits hosted in quartzite units in Islay formed from a fresh groundwater source (Nicholson, 1988), and that this is just one of many supergene Mn occurrences in that country (Nicholson, 1989). In South Africa, minor occurrences of Mn occur as vein-fillings and shear zone impregnations in coarse clastic units of the Waterberg Group (Eriksson et al., 1997), in quartzite units of the Pretoria Group of the Transvaal Supergroup, in the basal units of the Matsap Subgroup in the Olifantshoek Supergroup (Astrup and Tsikos, 1998), and in the quartz arenites of the Cape Supergroup. Of these South African deposits, these latter Cape Mn occurrences are the most extensive, and they have been most comprehensively evaluated in the national manganese review conducted by de Villiers (1960), and in the early work of Welsh (1917). The hosting Cape Supergroup sedimentary sequences were deposited in a rift basin (the Agulhas Sea) that formed between the Falkland Plateau and southern Gondwana, initiating at ~510 Ma. Termination of this sedimentation occurred around 350 Ma, and the Cape Supergroup was subjected to later deformation (last major deformation phase at 254 to 249 Ma; Blewett et al., 2019) to form the Cape Fold Belt. Based on Mn staining and cementing of poorly-consolidated recent talus, the mineralisation is suggested as being Neogene or Quaternary in age (Cole et al., 2014), although no direct geochronology has yet been conducted on these occurrences.

The most recent work on the Cape Mn occurrences has focused predominantly on structurally-hosted Mn deposits located on the Cape Peninsula on the far western margin of South Africa (Figure 1; Marchant, 1978; Theron, 1984; MacGregor, 2013; Killick, 2020). Here, the formation of noteworthy Mn occurrences is generally attributed to near-surface leaching of Mn and Fe from country rock, followed by re-precipitation in geological structures found preferentially in the quartz arenites of the Peninsula Formation. The deposits located further east within the Cape Fold Belt have been less well-studied and deserve a re-evaluation using modern analytical techniques and modern understanding of ore-forming processes. Importantly, in this eastern segment of the belt, several reports document instances of surficial manganese enrichment associated with chalybeate thermal springs (Kent, 1947; Gresse and Theron, 1992) yet their relationship with the structurally-hosted Mn mineralisation sub-type remains unresolved. These surficial accumulations bear some semblance to carbonate tufa, tavertine aprons and siliceous mounds associated with hydrothermal spring discharge elsewhere globally. However, because the mechanism of their formation is primarily by oxidation (versus e.g., decreasing CO_2 partial pressure in tufa accumulations) and because they have no genetic linkage to volcanic activity (but rather to artesian discharge under a hydraulic pressure gradient), we utilise the term 'Mn mound'.

The present study considers five structurally-hosted Mn deposits and eight manganiferous- and non-manganiferous thermal springs located in various parts of the Cape Fold Belt (Figure 1). The various study sites are considered from both a geological and a biogeochemical perspective using a range of analytical techniques and study approaches (optical microscopy, X-ray Fluorescence, X-ray Diffraction, aqueous geochemistry, isotope geochemistry, and microbiology). These results are combined and interpreted in a context of the ore geology 'mineral systems' framework (McCuaig et al., 2010) to provide a better understanding of the formation of the Mn occurrences, and to infer any possible inter-relationships between the two identified Mn deposit sub-types.

Methods

The sample set and the applied methodologies were broadly divided between those applicable to solid materials (microscopy and X-ray techniques) and those applied to the thermal spring waters (fluid physicochemistry, isotope systematics, microbiology, and PHREEQC modelling (Supplementary material) (Supplementary data files are archived in the South African Journal of Geology repository (https://doi.org/10.25131/sajg.127.0028.sup-mat)). The solid materials encompass structurally-hosted manganiferous vein infill and fault breccia impregnations (Bosjesmans, Dutoitskloof, Franschhoek, Rooiels, Simonsberg), as well as surficial, stratiform chemical precipitates or 'mounds' (Caledon, Towerwater, Warmwaterberg). The thermal spring water samples include four that are manganiferous (Warmwaterberg, Caledon, Towerwater, Calitzdorp), and as controls, a further four that are non-manganiferous (Brandvlei,

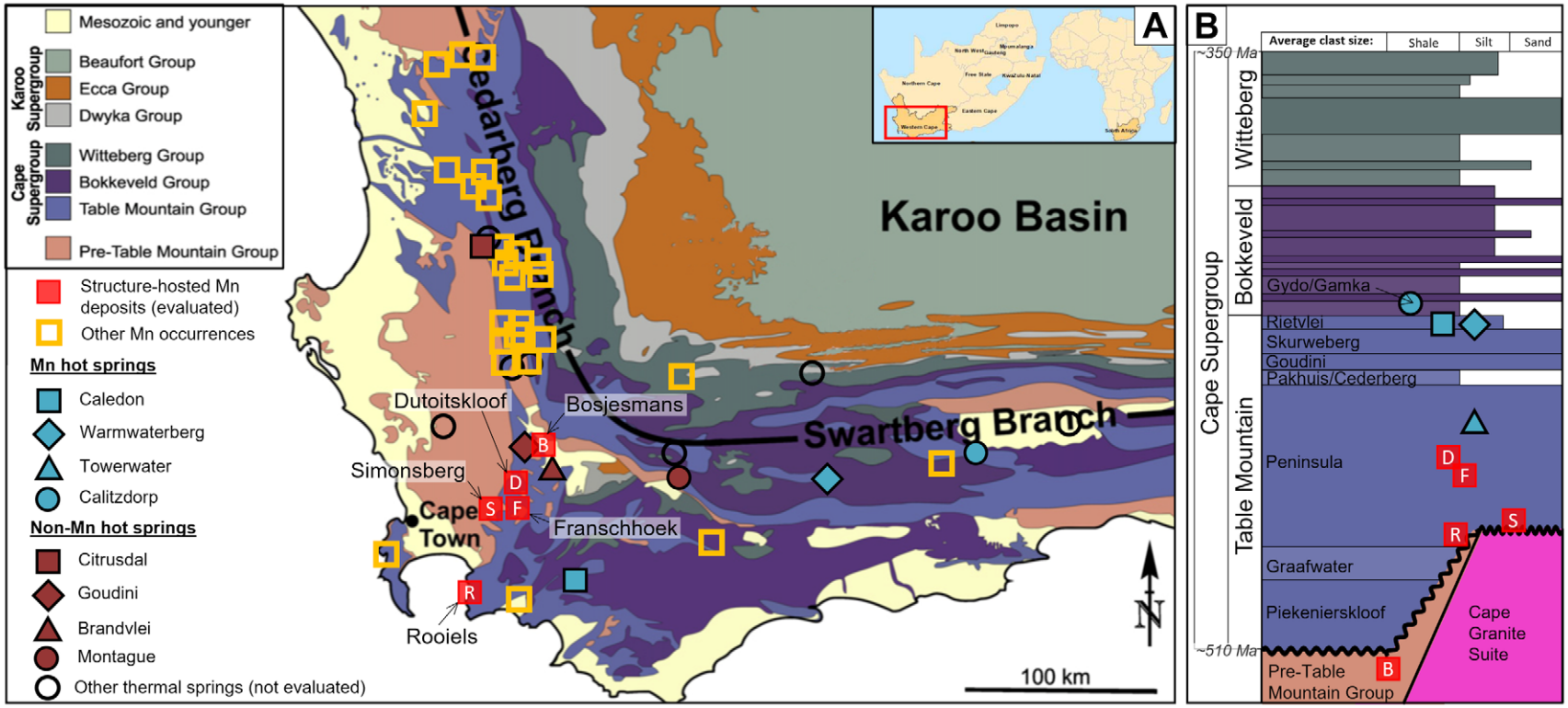

Figure 1 *(**A**) Spatial location of each hard rock and thermal spring sample evaluated in this study. Background map is adapted from Flint et al. (2011) and does not show the loci of Cape Granite Suite. Locations of other thermal spring occurrences are from Diamond and Harris (2000), locations of other Mn occurrences, which were not evaluated as part of this study, are from the Council for Geoscience. (**B**). Approximate stratigraphic position of each of the Mn samples considered in this study. The stratigraphic column with formation names and layer thicknesses is adapted from Thamm and Johnson (2006), whereas the age brackets are taken from Blewett et al. (2019) and references therein.*

Goudini, Montagu, Citrusdal). All the spring water samples are located in the Cape Supergroup rocks. The locations of each of these sampling sites are detailed in Figure 1a, and their relative stratigraphic positions are highlighted in Figure 1b.

Microscopy

A total of eight polished mounts and nine thin sections were prepared at the Central Analytical Facility (CAF; Stellenbosch University, South Africa) and Lab Crystals (India), respectively. All these mounts and sections were subject to detailed mineralogical and textural studies utilising a Zeiss Primotech® petrographic microscope employing transmitted light (to elucidate gangue mineralogy and textures) and reflected light (to evaluate the Mn and Fe assemblages). Magnification varied between 50x and 630x to ensure a multi-scale interrogation of each sample.

Whole-rock chemistry and mineralogy

Fifteen samples were ground to a fine powder (<20 µm) and then evaluated for their whole-rock chemistry using X-ray Fluorescence (XRF) and for their whole-rock mineralogy using X-ray Diffraction (XRD). These datasets were collected to provide complementary insights to the petrographic analyses described in the preceding section. The whole-rock datasets encompassed duplicate samples from most of the eight sampling sites, and inasmuch as these samples were selected to be as representative as possible, we acknowledge that the size of the sample set is insufficient to fully characterise the variability inherent in each Mn occurrence. Additional data reported in available literature were thus collated to help build out these datasets (Table 1).

The XRF analyses were conducted at the CAF on a PANalytical Axios WDXRF spectrometer and using the following standards for calibration: BE-N (basalt- from the International Working Group), JB-1 (basalt (depleted)), JG-1 (granodiorite), WITS-G (granite). The spectrometer is fitted with an Rh tube and with the following analysing crystals: LIF200, LIF220, PE 002, Ge 111 and PX1. The instrument is also fitted with a gas-flow proportional counter and a scintillation detector. The gas flow proportional counter contains a gas mixture comprising 90% argon and 10% methane. Major elements were analysed on a fused glass disk using a 2.4 kW rhodium tube. Matrix effects were corrected for by applying theoretical alpha factors and measured line overlap factors to the raw intensities measured with the SuperQ PANalytical software. The samples were milled to a fine powder after being oven dried at 40°C for 72 hours. Powdered samples were each mixed with high-purity trace element- and rare earth element (REE) free flux ($LiBO_2$ = 32.83%; $Li_2B_4O_7$ = 66.67%; LiI = 0.50%) to create fused glass beads for subsequent analyses. The major elements that were quantified as oxides include SiO_2, TiO_2, Al_2O_3, Cr_2O_3, P_2O_5, Fe_2O_3, MnO, MgO, CaO, Na_2O, and K_2O.

The XRD analyses were conducted at iThemba Labs in Cape Town, with measurements of samples taken using a multipurpose X-ray diffractometer D8-Advance from Bruker AXS, operated in a continuous Θ-Θ scan in locked coupled mode with Cu-Kα radiation. The powdered samples were mounted in the centre of the sample holder on a glass slide and raised to the correct height. The measurements run within a range of 2Θ as defined by the user with a typical step size of 0.034° in 2Θ. A position sensitive detector, Lyn-Eye, was used to record diffraction data at a typical speed of 0.5 seconds/step which is equivalent to an effective time of 92 seconds per step for a scintillation counter. The data were background subtracted so that the phase analysis for a diffraction pattern was carried out with zero background. Phases were identified from the match of the calculated peaks with those of the measured ones until all phases were identified within the limits of the resolution of the results.

Spring water sampling, physicochemistry and isotopic analyses

Of the eight springs sampled (Table 2), three coincided with sampling sites at which solid mound material was also sampled (i.e., Caledon, Towerater and Warmwaterberg; Figure 1). All water samples were collected within a short time frame between April and May 2021 to preclude any seasonality controls on the measured water signatures. Care was taken to ensure that sampling did not coincide with any major storm events. At each sampling site, two 100 ml samples were collected in polyethylene vials for subsequent laboratory-based physiochemistry and major ion analyses. Between collection and analyses, samples were stored in refrigerators at the BIOGRIP facility. Sample vials used for collecting the cation analysis samples were pre-acidified using Suprapur 65% nitric acid (Sigma-Aldrich). These samples, and those used for stable isotope analyses were filtered in the field using a 0.45 µm FilterBio CA syringe filters. The duplicate samples collected for ^3H and ^{14}C analyses were not filtered and were collected in 500 ml Azlon sample bottles. All vials were sealed immediately after being filled to prevent contamination and potential isotopic fractionation.

In situ field measurements were taken using ExTech's ExStik 2 EC500 probe to measure electrical conductivity (EC), total dissolved solids (TDS), salinity, pH and temperature. Laboratory measurements were taken at BIOGRIP, part of Stellenbosch University's CAF, to confirm the pH and EC readings. The BIOGRIP laboratory uses a Metrohm 930 Compact IC Flex, an Ion Chromatography instrument, in order to obtain concentration of major anions (Cl, F, NO_2, NO_3, PO_4, SO_4, and Br) and cations (Li, Ca, K, Na Mg and NH_4). The concentration of each of these ions was quantified using a conductivity and/or UV detector for the anions and a conductivity detector for the cations.

Stable isotope measurements were also done at BIOGRIP and utilised the Los Gatos GLA431-TLWIA triple liquid isotope analyser to determine stable isotope concentrations of oxygen and hydrogen. This machine vaporises the sample and from there uses the principles of spectroscopy to determine concentrations. The ^3H and ^{14}C were both analysed at the Institute for Nuclear Research (ATOMKI) in Hungary. The tritium samples were measured via the ^3He ingrowth method (Palscu et al., 2010). This is achieved by degassing of the sample and measuring the newly

Table 1. Semi-quantitative X-ray Diffraction (XRD) data (many poorly-crystalline oxide phases were not quantifiable by diffraction measurements i.e., X-ray amorphous) and X-ray Fluorescence (XRF) data for a small sub-set of sampled material from each site. Final two columns provide a synthesis of previously reported data.

Sample	Mangano-melane	Pyro-lusite	Nsu-tite	Verna dite	Fe oxides (Goethite ± Hematite)	Quartz	Al_2O_3	CaO	Fe_2O_3	K_2O	MnO	P_2O_5	SiO_2	L.O.I.	Other assays	Reference
Bosjesmans_A	36.0	21.9	6.0	25.7		10.3	2.9	0.1	4.5	1.3	70.0	0.6	3.0	16.2	22-43% Mn; 5-37% Fe; 0.5-2% P_2O_5	de Villiers, 1960
Dutoitskloof_A	14.5	38.9			24.9	21.7	1.8	0.1	24.7	1.5	56.6	1.2	2.5	11.8	36-46% Mn; 13-23% Fe; 0.4-0.5% P_2O_5	Welsh, 1917
Dutoitskloof_B	5.4	27.2			59.8	7.6	0.5	0.1	50.5	0.8	35.7	1.4	0.9	10.9		
Rooi Els_A	9.8				2.6	87.6	3.4	0.1	14.9	2.2	46.1	1.2	22.2	9.9	24-32% Mn; 11-20% Fe; 0.6% P_2O_5	Welsh, 1917
Rooi Els_B	0.7				0.2	99.0	2.9	0.0	2.5	0.7	10.2	0.1	79.3	3.9		
Franschhoek_A	9.9	21.8		6.7		61.6	1.9	0.2	0.9	2.4	75.0	0.8	7.8	11.3		
Franschhoek_B	9.2	27.7		6.2		56.9	4.3	0.1	1.5	2.4	66.7	0.7	12.0	11.6		
Simonsberg_A					94.8	5.2	1.8	0.1	80.2	0.0	0.3	3.7	0.8	13.0		
Simonsberg_B					10.2	89.8	1.4	0.0	53.1	0.1	3.3	3.2	27.9	11.2		
Towerwater_A					100.0		0.1	1.0	40.9	0.3	23.7	2.1	3.0	27.3		
Towerwater_B					80.2	19.8	0.4	0.2	68.1	0.0	0.4	2.1	12.1	16.8		
Warmwaterberg_A					53.2	46.8	0.4	0.2	50.2	0.1	18.2	1.1	19.7	10.8	9% Mn, 58% Fe, 1.2% P_2O_5	Kent, 1947; and
Warmwaterberg_B					66.6	33.4	0.3	0.3	46.2	0.2	27.3	0.6	10.3	14.4		references therein
Caledon_A	4.0				24.4	71.6	1.7	0.1	40.3	0.5	31.5	0.8	11.0	14.3	27% Mn, 51% Fe;2.3% P_2O_5	Kent, 1947; and
Caledon_B	6.8				83.0	10.1	0.6	0.1	65.8	0.3	13.3	2.5	1.7	14.7		references therein

Table 2. Physicochemical dataset for water samples collected from the manganiferous and non-manganiferous hot springs evaluated in this study.

	Physicochemistry					**Major elements**									
	Cond. (µS/cm)	**Temp. (°C)**	**pH**	**TDS (mg/L)**	**Flow.[a] (l.s^{-1})**	**Ca (mg/L)**	**Mg (mg/L)**	**Na (mg/L)**	**K (mg/L)**	**Cl (mg/L)**	**SO_4 (mg/L)**	**CO_3^{2-} (mg/L)**	**HCO_3^- (mg/L)**	**P (mg/L)**	**Si (mg/L)**
Caledon	194.6	47.5	6	115.5	10	7.78	3.17	17.24	4.88	34.01	4.26	30.3	0	<LOD	25.20
Warmwaterberg	254	43.2	6.81	154	5	15.71	2.66	19.87	8.64	31.79	4.42	55.4	0	<LOD	22.94
Towerwater	208	41.6	6.24	119.2		12	3.54	12.51	6.78	24.46	3.18	41.1	0.2	<LOD	15.49
Calitzdorp	224	46.5	6.4	129		9.99	4.43	15.46	8.33	33.19	5.41	30	7.5	<LOD	18.94
Citrusdal	75.3	41.9	5.66	46.2	30	2.77	2.06	7.85	1.92	15.44	<LOD	11.1	0.2	0.19	11.29
Goudini	72.94	40.8	6.3	80.7	3	7.14	1.80	5.19	0.96	11.13	1.68	16.9	0	0.23	13.89
Brandvlei	73.34	51.1	5.93	54	126	4.10	2.15	7.14	1.95	14.11	1.46	12.2	0.6	0.20	18.10
Montague	133.6	37.8	6.95	80.7		11.18	2.75	8.54	3.70	17.16	2.32	32.6	0	0.17	13.72

	Trace elements														
	Mn (µg/L)	**Fe (µg/L)**	**B (µg/L)**	**V (µg/L)**	**Co (µg/L)**	**Ni (µg/L)**	**Cu (µg/L)**	**Zn (µg/L)**	**As (µg/L)**	**Se (µg/L)**	**Sr (µg/L)**	**Mo (µg/L)**	**Cd (µg/L)**	**Sb (µg/L)**	**Ba (µg/L)**
Caledon	4183.72	207.65	14.29	0.03	1.13	0.22	<LOD	0.75	0.72	0.01	41.32	0.04	<LOD	0.02	96.01
Warmwaterberg	993.42	1156.16	30.14	0.02	0.13	0.16	<LOD	1.93	1.29	<LOD	190.28	0.12	<LOD	0.27	230.49
Towerwater	1824.63	65.68	24.81	0.03	0.11	0.08	<LOD	0.65	0.24	<LOD	136.50	0.17	<LOD	0.06	132.35
Calitzdorp	2744.21	27.51	26.98	0.02	<LOD	0.22	<LOD	2.85	0.24	0.01	77.17	0.18	<LOD	0.02	100.76
Citrusdal	1.32	<LOD	9.60	0.67	0.01	0.46	<LOD	2.87	0.38	0.11	4.96	0.03	0.01	<LOD	4.90
Goudini	0.40	<LOD	4.67	0.46	0.01	0.15	1.23	2.49	0.67	0.06	20.74	0.03	0.01	0.01	3.64
Brandvlei	0.50	<LOD	7.54	1.29	0.05	0.78	0.24	10.11	0.45	0.06	14.79	0.06	0.02	0.01	12.54
Montague	0.13	<LOD	10.39	1.33	0.29	2.31	1.24	14.39	1.07	0.06	86.85	0.07	0.02	0.02	16.47

	Isotope geochemistry			
	δD	**$\delta^{18}O$**	**^3H (TU)**	**Radiocarbon age (years)**
Caledon	-22.4	-4.9	0.042	5914
Warmwaterberg	-38.8	-6.89	0.090	14902
Towerwater	-36.8	-6.58	0.028	5371
Calitzdorp	-39.5	-6.91	0.014	11774
Citrusdal	-23.2	-4.6	0.117	2994
Goudini	-27.3	-5.1	0.224	2506
Brandvlei	-33.6	-5.94	0.064	2599
Montague	-30.6	-6.12	0.027	4819

[a] Flowrate measurements taken from Diamond and Harris (2000)

produced ^3He from tritium decay using a dual collector (noble gas) mass spectrometer (van Rooyen et al., 2020). The ^{14}C samples were analysed using the EnvironMICADAS accelerated mass spectrometer (AMS) with a gas ion source. Radiocarbon ages were calculated using the standard radioactive decay equation, with the assumption that modern recharge has the same ^{14}C value as local modern rainfall (van Rooyen et al., 2022). No correction was applied for the dissolution of carbonate rocks because the regional geology contains very few carbonate sources, and because the water samples have ^{13}C abundances that are consistent with local soils, thus suggesting a negligible contribution of 'dead carbon' to the spring waters.

Microbiology investigations

The microbiological sample set consisted of water samples, and associated sediment and microbial mat samples. Water samples were collected at all eight of the thermal springs following the sampling protocols described in the preceding section. At sampling sites where sediments (Towerwater, Warmwaterberg, Citrusdal and Calitzdorp) and/or floating microbial mats (Brandvlei and Calitzdorp) were accessible, these too were collected for microbiological characterisation (DNA extraction and sequencing).

Community DNA was extracted from the water, sediment and microbial mat samples collected at each thermal spring using the ZR Quick-DNA Fecal/Soil Microbe Kits (Zymo

Research). For the water samples, approximately 500 ml of water was filtered through a sterile 0.22 µm filter. Each filter was shredded into smaller pieces and transferred to a 2 ml Eppendorf tube containing the bashing bead solution buffer and 0.425 mm acid washed glass beads. Each tube was shaken on a Disruptor Genie for 15 minutes before transferring the solution buffer containing the microbial cells to the bashing bead tube. For the sediment and microbial mat samples, at least 500 mg of the sample was added to the bashing bead tube with the solution buffer. All DNA extractions were performed following the manufacturer's instructions. The extracted DNA was stored at -20°C. PCR amplification of the extracted DNA was performed according to Conradie and Jacobs (2021). Primers 319-F (5'-ACTCCTACGGGAGGCAGCAG-3') and 783R (5'- CTACCAGGGTATCTAATCCTG-3') were used to target the 16S rRNA gene V4-V5 region. The reaction volume for each PCR contained 0.5 U KAPA Taq HotStart DNA Polymerase, 1x KAPA Taq Hotstart Buffer, 0.5 µl of a 10 mM dNTP mix, 1.5 mM $MgCl_2$, 0.25 µM forward and reverse primers, and 1.5 µl of template DNA to a final volume of 25 µl. PCR amplifications were performed on a 2720 Thermal Cycler (Thermo Fisher Scientific) with an initial denaturing of the DNA at 95°C for five minutes, followed by 95°C for 30 seconds, 58°C for 30 seconds and 72°C for one minute, for 35 cycles. A final extension at 72°C for one minute was completed and the PCR samples were held at 4°C until further processing. Each sample was done in triplicate and pulled before library preparation. Samples were loaded onto an Ion 530™ Chip for sequencing using the Ion S5 Sequencing Systems (Ion Torrent, Thermo Fisher Scientific) at the CAF Stellenbosch University.

The raw sequence data (BAM files) were converted to FASTQ files and analysed using Mothur v.1.48.0, following the 454 tutorial available at http://www.mothur.org/wiki/, with some modifications (Schloss et al., 2009). Sequences were trimmed and aligned against the recent SILVA v.138.1 bacterial reference database (http://www.arb-silva.de/). Chimeric sequences were removed with the chimera.uchime command (Edgar et al., 2011) and the remaining quality filtered sequences were classified using a cut-off value of 80. Classified sequences were clustered into operational taxonomic units (OTUs) and each sample was normalised to 7506 sequences. Following normalisation, all statistical analyses were performed in R (v.4.1.1, R Core Team 2013) using the microeco package (Liu et al., 2021). For the identification of potential biomarkers, the LEfSe method was implemented. A p-value of ≤0.05 was considered as significant for all statistical measurements.

Selected Western Cape Mn occurrences

Outside of the early works of Welsh (1917), de Villiers (1960) and a review by Cole et al. (2014; and references therein), most of the available scientific literature has focussed predominantly on Mn occurrences on the Constantia Massif (Marchant, 1978; Theron, 1984; MacGregor, 2013; Killick, 2020). The present study expands on this body of work by considering some of the less-studied occurrences within the Western Cape (Figure 1). Table 1 summarises the XRF data and XRD data for the respective Mn occurrences, including a collation of historically published data. The occurrences are described in order of the structurally-hosted sub-type first, then the stratiform mound deposits.

Dutoitskloof

The Dutoitskloof Mn vein is located above the eastern entrance to the Dutoitskloof tunnel and was exploited for manganese in the 1870's – 1880's (Figures 1 and 2a and Cole et al., 2014). It is regarded as the largest Mn deposit in the Drankenstein and Hottentots Holland area (Gresse and Theron, 1992), where it is hosted in a ~300 m long steeply-dipping fault zone that crosscuts the bedding of the Peninsula Formation sandstone units. The host structure has a strike of ~140°, which is roughly parallel to several mapped faults in the Elandspadrivier Valley (Figure 2a). The main mineralised vein attains a maximum thickness of 3 m and is flanked by a set of narrower parallel-striking Mn veins. These veins are competent and weather positively with respect to the sandstone host lithology, and the main veins carry a gun-metal blue colour indicative of crystalline Mn oxides such as pyrolusite. Adjacent to the veins, Mn has also stained the sandstone, predominantly replacing the cement between individual quartz veins. Breccia in-fill and open-space botryoidal Mn growth textures are prevalent. For the two samples analysed, the XRF data indicate MnO content of 35 to 57 wt.%, in broad agreement with previous assays of 36 to 46 wt.% Mn (Welsh et al., 2017; Table 1). The XRD measurements reveal the presence of manganomelane minerals, pyrolusite and iron oxides (Table 1), which show textural evidence of open-space filling (Figure 3a to g).

Bosjesmans

A steeply dipping Mn-rich vein is located on the Bosjesmans Valley farm 218, where it represents a unique occurrence of Mn in phyllitic units of the Norree Formation of the Malmesbury Group (Figures 1, 2b; Gresse and Theron, 1992). The site is situated approximately 4 km north of the main splay of the large Worcester Fault, in rocks that have experienced both folding and slip. Historical mining has exploited 22 to 43% Mn ore to a depth of about 5 m (de Villiers et al., 1960; Gresse and Theron, 1992). Although higher grade material exists in some of the waste piles, *in situ* manganiferous material is low grade, friable and commonly cross-cut by 1 to 5 mm thick conjugate intersecting sets of carbonate veinlets (Figure 2b). The ore zone grades outwards into a zone of Fe enrichment and then into the weathered kaolinite-containing wall rock. The XRD results of the ore revealed the presence of cryptomelane, pyrolusite and poorly crystalline nsutite and vernadite minerals.

Franschhoek

The Franschhoek locality has many broad similarities with the Dutoitskloof mineralisation, comprising predominantly manganomelane minerals as infill in sandstone breccia, or occurring as positively-weathering vein arrays, or as impregnations or cement-replacement within the adjacent sandstone wall rock (Figure 3). These altered wall-rocks typically

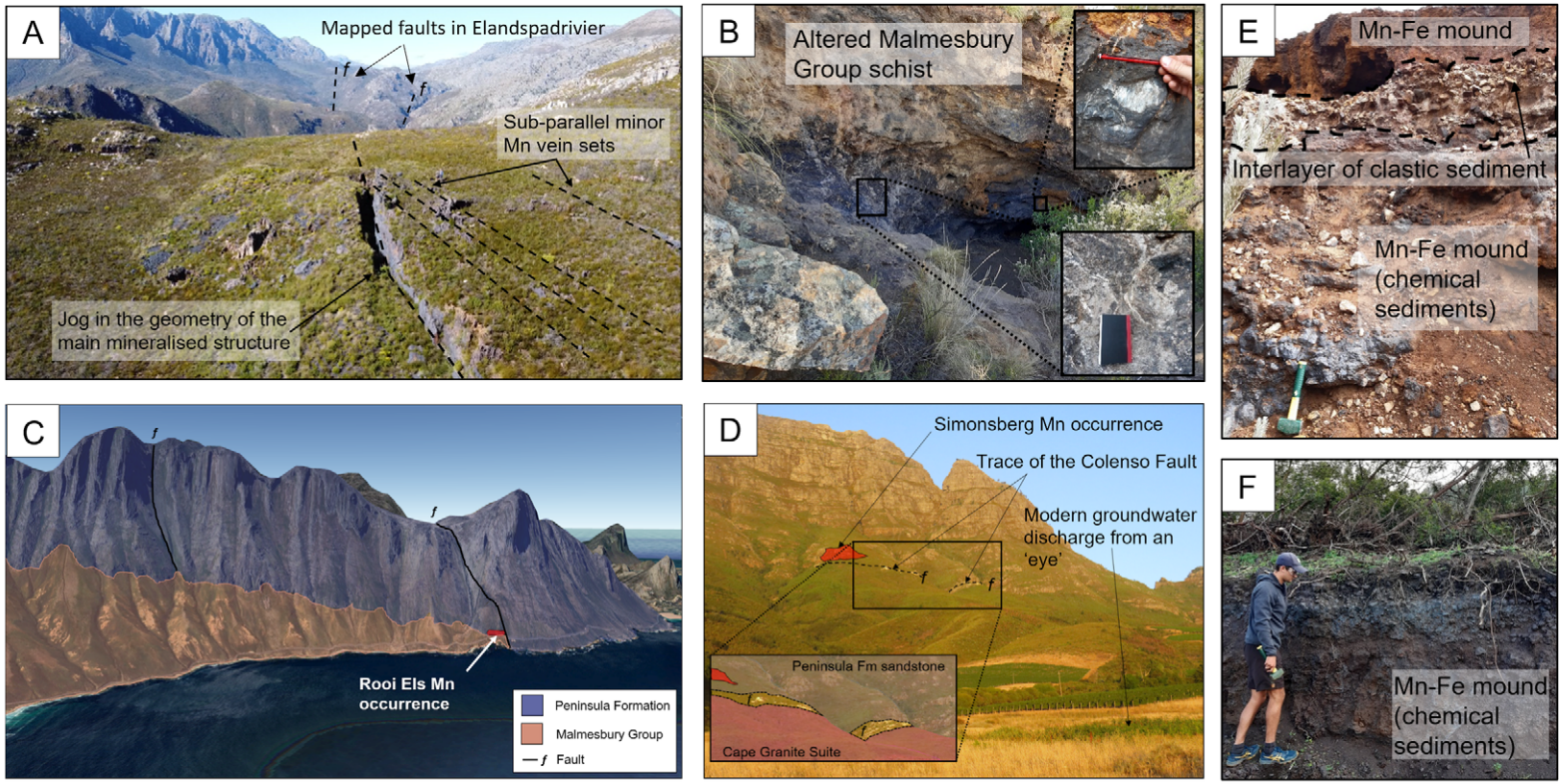

Figure 2. *Field relationships observed at several selected Mn study sites. (**A**) Oblique view (looking SE) of the main mineralised fracture and associated sub-parallel vein sets at the Dutoitskloof Mn deposit. (**B**) A historically-mined Mn deposit at the Bosjesmans wedding venue where Mn is hosted in Malmesbury group metasediments. Inset photos (slickensides (top) and cross-cutting carbonate vein arrays (bottom)) highlight the structural complexity of the site, which is located near to the regional-scale Worcester Fault. (**C**) Oblique view Google Map imagery showing the location of the Rooiels Mn occurrence and its intimate relationship with a mapped northwest-southeast striking fault and close spatial proximity to the underlying, low-permeability Malmsbury Group metasediments. (**D**) Location of the Simonsberg Mn occurrence in the basal layers of Peninsular Formation sandstone, and above the low-permeability silicified granites formed through metasomatic activity along the Colenso Fault (outcropping fault trace is annotated). (**E**) Interlayering of chemical sediment (Mn-Fe ± Si mound) with clastic breccias from surrounding Cape Supergroup slopes at the Towerwater thermal spring. (**F**) Layering in the Mn-rich mound at the Caledon thermal spring suggests post-depositional remobilisation of metals by diagenetic and supergene processes.*

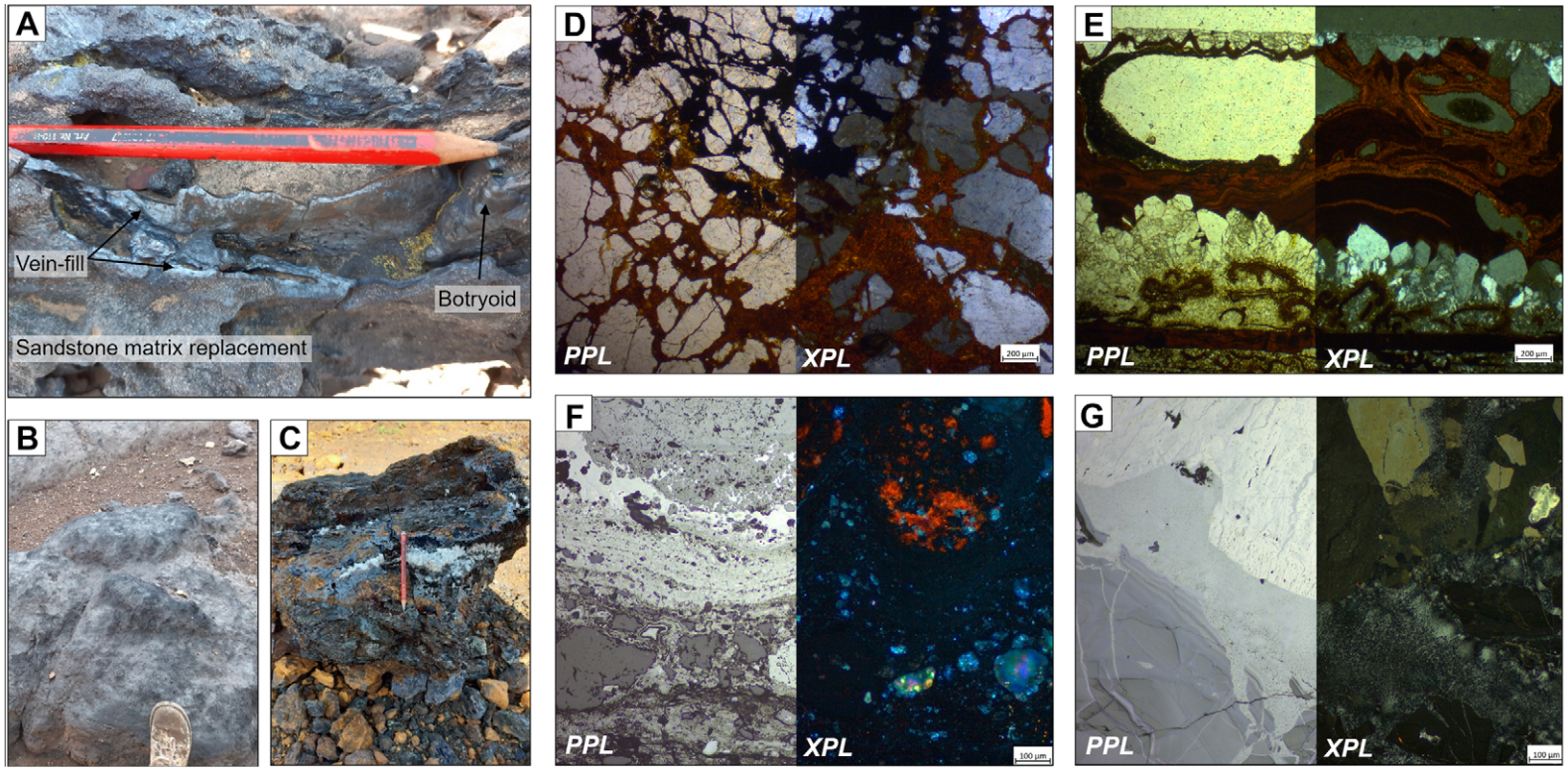

Figure 3. *Selected hand sample and microscopic images (PPL = plane-polarised light; XPL = crossed-polars) of mineralisation textures. (**A**) Vein and sandstone replacement type textures observed in outcrop at the Dutoitskloof Mn deposit. (**B**) Low grade Mn mound material at the Towerwater thermal spring. (**C**). Complex mineralogy showing Mn- and Fe oxides and oxyhydroxides and late calcite precipitates in mound material from the Caledon thermal spring. The localised calcite likely forms from downward percolating meteoric water that intersects open-spaces developed in the accumulated mound material. (**D**) Transmitted light micrograph showing preferential replacement of the sandstone matrix relative to the individual quartz grains. Apparent zonation between Mn (black) and Fe (red) may be caused by a redox gradient Fe precipitates at lower Eh relative to Mn). (**E**) Transmitted light micrograph showing open space filling textures: syntaxial quartz crystals overgrown by concentric bands of Fe-Mn oxides. Cuspoid shaped oxide minerals at the bottom of the micrograph may represent replacement of organics. (**F**) Reflected light micrograph of mound material from the Caledon thermal spring highlighting the very fine crystallite sizes and concentric growth banding. (**G**) Reflected light micrograph of coarser-grained Mn mineralisation (pyrolusite and manganomelane minerals) from the structure-hosted deposit at Dutoitskloof. Brittle fracturing, and infill by successive generations of Mn minerals, suggests multiple activations of the host structure.*

carry a purplish colour indicating a mix of both Fe and Mn oxides in the replacement assemblage. The main hosting structure, found in a prominent saddle in the Mont Rochelle Nature Reserve, is located within Peninsula Formation sandstone and strikes northwest for approximately 100 m (de Villiers et al., 1960). Most of the *in situ* veins attain a maximum thickness of ~5 cm, although piles of historically-mined material include more massive samples. Mineralogical analyses suggested the presence of several Mn^{4+} minerals, and a strong signature of the quartz rich wall-rock, whereas XRF measurements additionally highlighted the presence of Fe oxide minerals and low (<0.9 wt.%) phosphate contents (Table 1). This corroborates earlier work which suggested that the ore is ferruginous, low in phosphate, but with noteworthy instances of lithiophorite ($(Al,Li)MnO_2(OH)_2$) and minor amounts of Co and Li (de Villiers et al., 1960 and references therein).

Rooiels

The Rooiels occurrence is hosted in sandstone in a road cutting on Clarens Drive between Kogel Bay and Rooiels (Figure 2c). The main outcrop is located towards the base of the Peninsula Formation, above a nonconformity contact with underlying greenschist facies Malmesbury metasediments which may have acted as a significant aquiclude. It is also adjacent to a mapped normal fault that juxtaposes these two lithologies against one another in a lateral sense (Figure 3c). Primary sandstone textures are still observable within most of the main outcrop, which carries a dull black colour. However, upon sampling, the Mn enrichment is revealed to be relatively superficial, with underlying sandstone host comprising predominantly quartz grains and iron staining. This is reflected in the typically low grades reported in both the current and historical datasets (Table 1). Higher-grade samples represent manganiferous veins which sometimes show botryoidal textures, and which commonly grade outwards into a yellow-orange-red alteration zone comprising various iron oxides.

Simonsberg

A relatively minor occurrence of Mn is located in Peninsula Formation sandstones about halfway up the Simonsberg and just above a nonconformity contact with the underlying Cape Granite Suite. The main Mn outcrop has a maximum width of ~4 m and length of ~10 m, although thin Mn-bearing structures continue along strike for a further ~50 m. Importantly, the siting of the mineralisation is proximal (within 100 m) of a prominent exposure of silicified and epidotised granite (Figure 3d), which represents the trace of the long-lived (>500 Ma) Colenso Fault system (Kisters et al., 2002). This co-occurrence is conspicuous and suggests that both formed (albeit at vastly different times) in a mutual jog structure associated with the still-active Colenso fault, or that the silicified fault zone has acted as an efficient aquiclude directing more recent ground water flow laterally (i.e., as described for the Rooiels occurrence). The sampled hand specimens were predominantly ferruginous, and returned poor Mn concentration values and poor Mn mineral abundances (Table 1). However, macroscopic and microscopic observations revealed complex quartz - Mn oxide intergrowth textures (Figure 3e).

Mn mound deposits (Caledon, Towerwater and Warmwaterberg)

Stratiform mound deposits (Figures 2e and f; 3b, c and f) are associated with three chalybeate thermal springs discharging at surface within the confines of the Cape Fold Belt, and have been previously described to a limited extent by Kent (1947). The largest of these is the Caledon mound which has been estimated to contain 250 kt ore grading at up to 40% Mn (de Villiers, 1960). The Warmwaterberg mound is estimated to be about half the size of the Caledon deposit (Kent, 1947 and references therein), whereas the size of the Towerwater occurrence has not been estimated, though it has a relatively large surface expression measuring in excess of 10 000 m^2. At each deposit, the iron and manganese oxides and -oxyhydroxides that concentrate in mounds display variable textures and colours. The majority of the material is quite dull, friable, earthy and brown-black, with zones of red-orange ferruginous material. More competent lenses and linear structures may contain metallic-to-submetallic lustres, blue-black colouration, and discernible botryoidal and stalactite textures (Figure 3c). Locally, infiltrating meteoric water has resulted in precipitates of carbonate minerals (Figure 3c), and at Towerwater, surficial erosion processes have led to interspersed clastic breccia lenses and fluvial incision of the mound (Figure 2e), possible due to recent geomorphic uplift (e.g., Partridge and Maud, 1987). The poorly crystalline nature of the mound deposits hampered the use of XRD for mineralogical investigation (Table 1), where predominantly Fe oxides were identified. From XRF measurements however, the MnO concentrations of the respective sites ranged up to 23 wt.% (Towerwater), 27 wt.% (Warmwaterberg), and 32 wt.% (Caledon). These data compare favourably with those in Kent (1947) who reported 27 wt.% Mn in samples from Caledon and 9 wt.% Mn in samples from Warmwaterberg.

Manganiferous and non-manganiferous thermal springs

The results for the extensive set of biogeochemical investigations conducted on the spring water samples are best presented in a comparative manner in which the characteristics of manganiferous springs are contrasted with those of the non-manganiferous springs (Table 2; Figures 4 and 5). Three of the manganiferous thermal springs (Caledon, Warmwaterberg and Towerwater) were associated with manganiferous and ferrous mound deposits described in the preceding section. The Calitzdorp thermal spring is located directly next to (effectively on the flood plain of) the relatively large Olifants River, and this siting has negated the development or preservation of an appreciable mound deposit.

Physicochemistry results

The electrical conductivity (EC) data ranged between 194 and 254 for the manganiferous thermal springs, and between 75

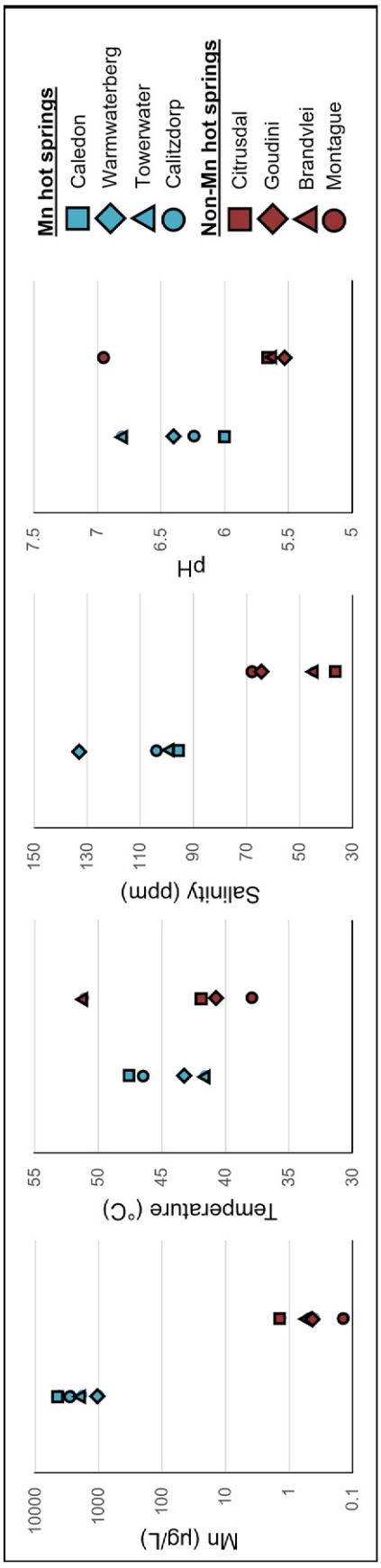

Figure 4. *Comparative graphs detailing some of the differences in the physicochemical properties of the manganiferous versus the non-manganiferous thermal springs.*

and 138 for the non-manganiferous thermal springs (Table 2). The highest EC values were measured in the Warmwaterberg thermal spring, which also had the highest salinity and TDS measurements. The Brandvlei thermal spring had the lowest measured EC value (91 µS/cm), although Citrusdal showed the lowest salinity and TDS measurements (Figure 4). All pH measurements were mildly acidic and fell within the range of 5.53 and 6.95 (Table 2). The highest pH values were measured in the Montagu non-manganiferous thermal spring, although the subset of manganiferous thermal springs on average (avg. 6.36 ± 0.29 (one standard deviation)) have higher pH than the more acidic non-manganiferous subset of thermal springs (avg. 5.70 ± 0.15). The trends in the salinity and TDS measurements followed that of the EC measurements (Figure 4), with manganiferous thermal springs characterised by statistically significant higher values (student t-test; $p = 0.05$) than their non-manganiferous counterparts. The overall range in salinity was between 37 and 133 ppm, and the overall measured range in TDS was between 46 and 154 (Table 2 and Figure 4).

The major element concentrations in each water sample are detailed in Table 2 and shown as Stiff diagrams in Figure 5. These representations indicate that univalent cation grouping (Na^+ and K^+) is quantitatively more important than the individual divalent cations (Ca^{2+} or Mg^{2+}), except in the Goudini and Montagu non-manganiferous springs where Ca^{2+} is most abundant. Chloride is the dominant anion in 50% of the sites evaluated (Caledon, Calitzdorp, Brandvlei and Citrusdal), and at the remainder of the sites the summed value of bicarbonate and carbonate ion concentration dominates the anionic component of the water chemistry. Sulphate is the least important anion and its concentration never exceeds 0.2 milliequivalents per litre. Importantly, the shapes of the manganiferous thermal spring Stiff diagrams are consistently broader than those of the non-manganiferous thermal springs (Figure 5), corroborating and explaining the TDS, EC and salinity results.

Isotope and age results

Stable isotopes of O and H (reported as $\delta^{18}O$ and $\delta^{2}H$) are compared to data collected from local groundwater wells in the region (van Rooyen et al., 2021) as well as modern precipitation values from local weather stations (Table 2 and Figure 6), including the local (Harris et al., 2010) and global meteoric water lines. Water collected from the thermal springs generally had the most depleted signatures, whereas local (shallower) ground waters were more enriched and trended toward mean weighted averages of local precipitation in the region. Neither groundwater nor springs presented evaporation trends, suggesting recharged waters are derived in the cooler winter months and occur as direct recharge, rather than from lakes and rivers, consistent with regional groundwater recharge studies (van Rooyen et al., 2021; Harris, 2023). Furthermore, D-excess values are consistent with local rainfall trends of more arid vapour sources over the Southern Ocean, suggesting recharge waters are derived from late Holocene precipitation post the Antarctic Cold Reversal (14 kya) and the last glacial maximum (19 kya). Groundwater samples appear to cluster in two groups, one more associated

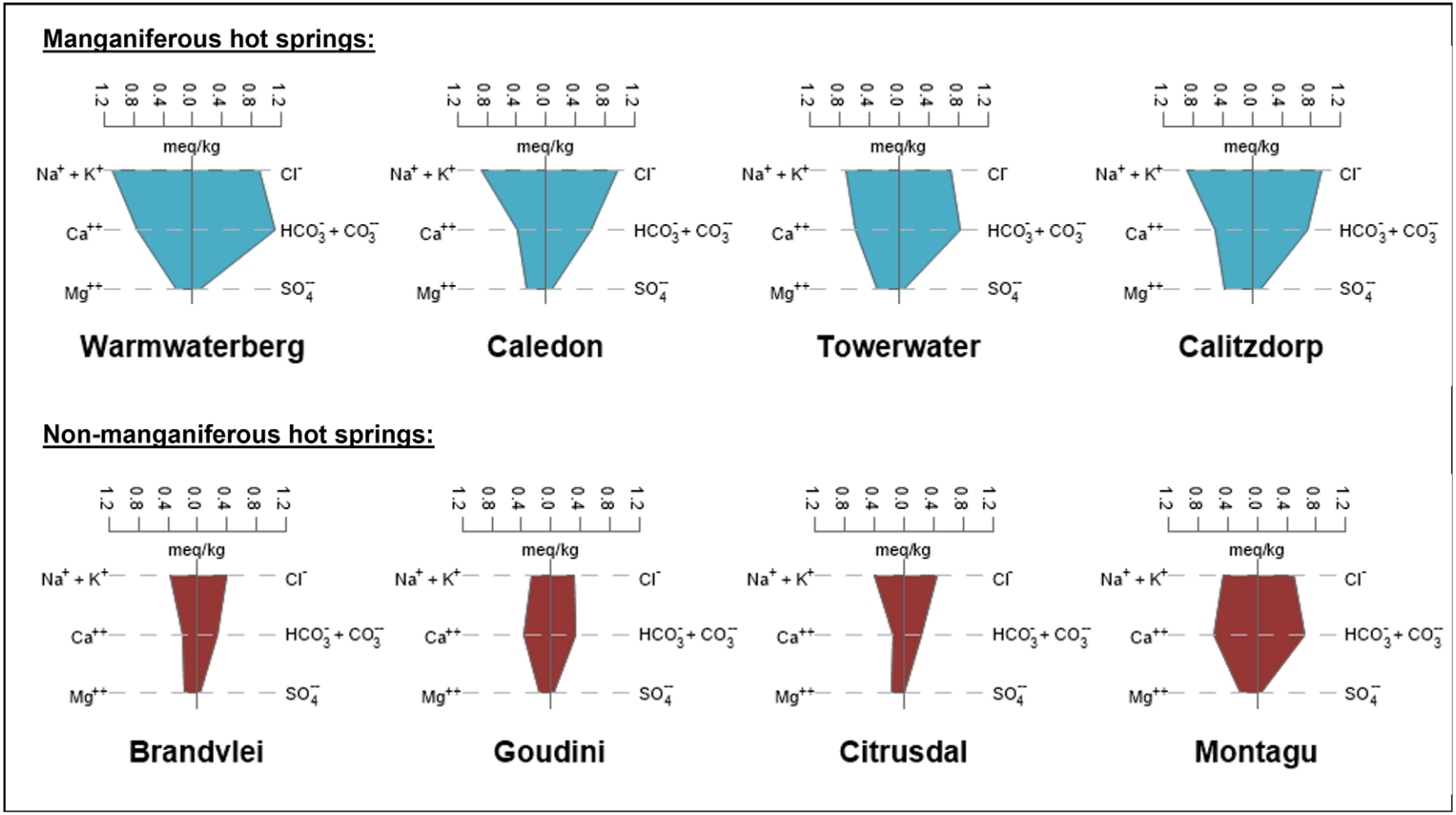

Figure 5. *Stiff diagrams comparing the major element chemistry for water samples collected from the manganiferous thermal springs versus those collected from the non-manganiferous thermal springs.*

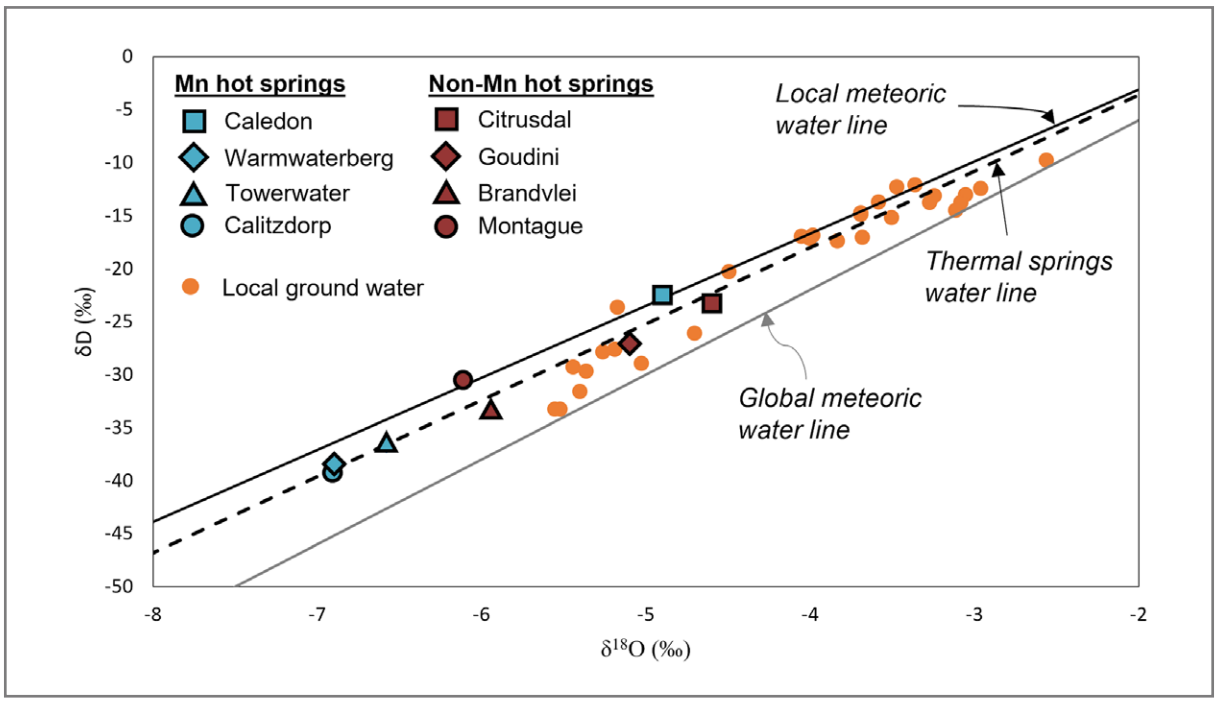

Figure 6. *Binary plot showing the δD versus $\delta^{18}O$ stable isotope signatures for the various spring water samples evaluated in this study. These data are compared against the stable isotope signatures of local ground waters (van Rooyen et al., 2021) and against global- and local- (Harris et al., 2010) meteoric water lines. Dashed line represents the thermal springs water line obtained from a linear best-fit of our data (equation: y = 7.2013x + 10.818; r^2 = 0.95).*

with modern precipitation values and the other more akin to spring waters, potentially mixing with deeper older groundwaters.

The mixing of multiple groundwater sources in spring waters is consistent with radiogenic isotope data, represented by groundwaters with a large range of radiocarbon ages containing measurable tritium (Figure 7). Springs that had the oldest radiocarbon ages (>5 000 years old) contained the lowest abundance of tritium, suggesting the mean residence time of these groundwaters reflects a larger portion of older groundwaters that are potentially derived from deeper systems. In general, all springs had low tritium abundances with local rainfall estimated to have levels between three and five TU and spring waters samples only containing 0.1 to 0.3 TU i.e., an order of magnitude lower than that of modern precipitation. Such low tritium values are likely a result of spring waters containing <10% of modern groundwater or simply a result of the *in-situ* production of tritium through rock water interaction, e.g., the production of ^3H through U-Pb decay (Andrews and Kay, 1982). In general, radiocarbon ages correlate with temperature where older groundwaters (with lower ^3H abundances) have higher discharge temperatures at the spring source. The exception is at the relatively high-temperature Brandvlei spring where radiocarbon ages are younger, though still reflecting ages of >2 000 years before present. These manganiferous springs are also typically older (average age: 9 490 ± 4 628 years before present (ybp)) than the non-manganiferous springs (3 230 ± 1 080 ybp).

Microbial diversity and composition

Microbial diversity was classified at phylum level for all sample types (microbial mat, sediment, and water). Family level classifications were used to describe the microbial diversity of only the water samples. The different taxa are represented as a percentage based on their relative abundance for the manganiferous and non-manganiferous groups (Figure 8a). Several phyla were observed in the thermal springs, with the most abundant phyla being Proteobacteria (63.1%), Firmicutes (9.7%), Acidobacteriota (8.9%), Bacteroidota (7.9%), and Actinobacteriota (4.8%) across all samples. The phyla represented by each sample type are similar, however, their composition varies between the Mn and non-Mn groups. At the family level, differences were observed between the two groups (Figure 8b). For the manganiferous groups the dominant families are the Sphingomonodaceae, Chromobacteriaceae, Oxalobacteriaceae, and the Comamonadaceae whilst for the non-manganiferous group the most dominant families are Pseudomonodaceae, followed by Sphingomonodaceae.

Alpha-diversity describes the species richness or evenness or both within a community (Fisher et al., 1943; Shannon, 1948; Simpson, 1949). The alpha-diversity indices measured, inferred a higher species richness and evenness for the manganiferous water samples, compared to the non-manganiferous water samples, with Shannon and Simpson indices of 2.54 and 0.93 respectively (Table 3). However, these indices were determined to not be significant (p>0.05). In a Principle Component

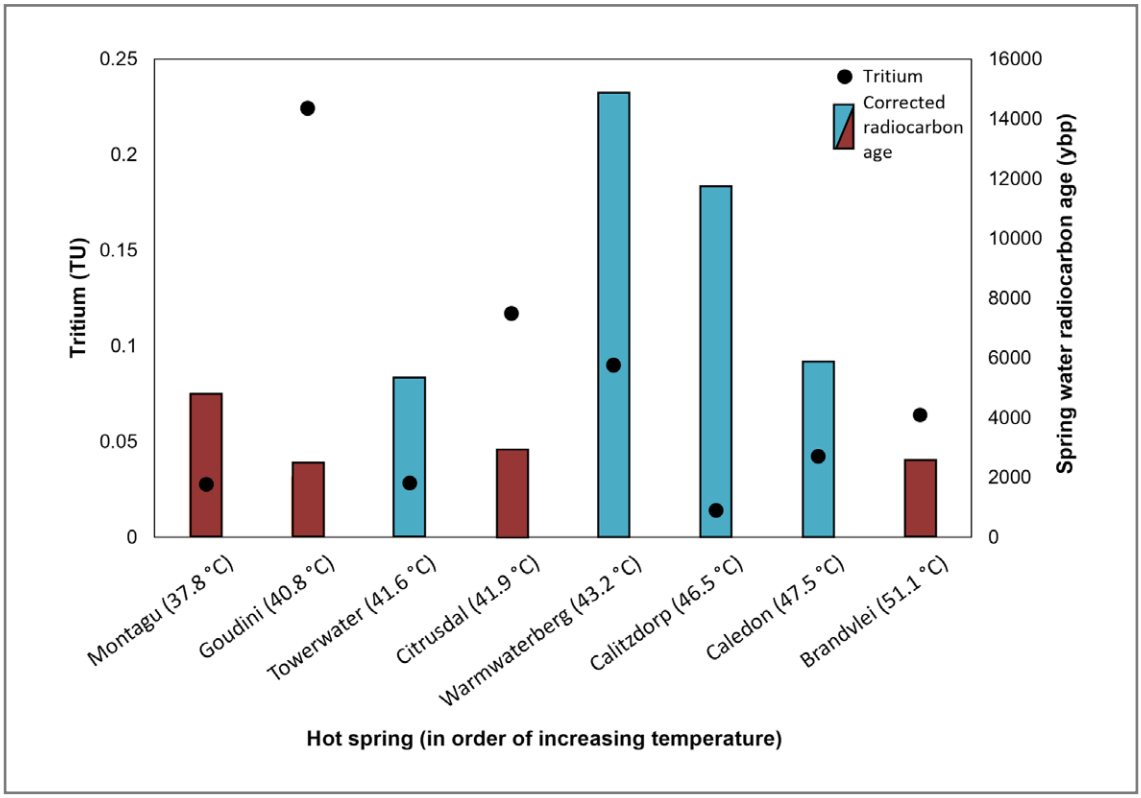

Figure 7. *Plot detailing the tritium concentrations and the radiocarbon ages (ypb=years before present) for spring water samples evaluated in this study. Springs are ordered according to increasing temperature, and bar colours reflect manganiferous springs (blue) versus non-manganiferous springs (maroon).*

Table 3. Alpha-diversity indices of the manganiferous and non-manganiferous water samples, including Observed Operational Taxonomic Units (OTU), Shannon and Simpson's indices. Values are means ± standard deviation. OTUs indicate the number of genera observed. Shannon index is used to observe richness and evenness. A higher Shannon value indicates a higher diversity. Simpson's index describes the microbial evenness. Values fall between 0 and 1. A Simpson's value close to 1 indicates an evenly distributed community, whereas a value closer to 0 indicates dominance of one or more microorganisms.

Group	Observed OTU	Shannon	Simpson
Water Mn	358 ± 116	2.54 ± 1.02	0.93 ± 0.25
Water Non-Mn	332 ± 221	1.50 ± 1.32	0.43 ± 0.38

Analysis (Supplementary material), the PCo1 and PCo2 axes represented 17.6% and 30.9% variance, respectively. The clustering of the different sample groups appear separate, suggesting that there is notable beta-diversity (amount of differentiation between communities) between the different groups. Further, the linear discriminant analysis (LDA) effect size was used to identify significant operational taxonomic units (OTUs) across groups (Figure 8c). In total, sixteen OTU taxa were identified as being significant. These included in the manganiferous group the orders Ignavibacteriales, Azospirillales, and Burkholderiales, families Azospirillaceae, Rhodocyclaceae, Gallionellaceae and Oxalobacteraceae, and genera *Ramlibacter*, *Azohydromonas*, and *Azospirillum*. In the non-manganiferous group, the order Rickettsiales, family Streptococcaceae, and genera *Streptococcus* and *Granulicella* were significantly represented.

Discussion

Genetic links between mound-type and structurally-hosted Mn occurrences?

Multiple classification schemes have been used to describe Mn enrichments in earth's crust (e.g., Laznicka, 1992; Roy, 1997). In the local context, early workers have described the Mn occurrences as either gash-type veins, sandstone impregnations or fault/breccia infill (de Villiers, 1960; Theron, 1992). This has recently been expanded on by Killick (2020) who suggests that saprolite (from weathered doleritic dykes) replacement may be

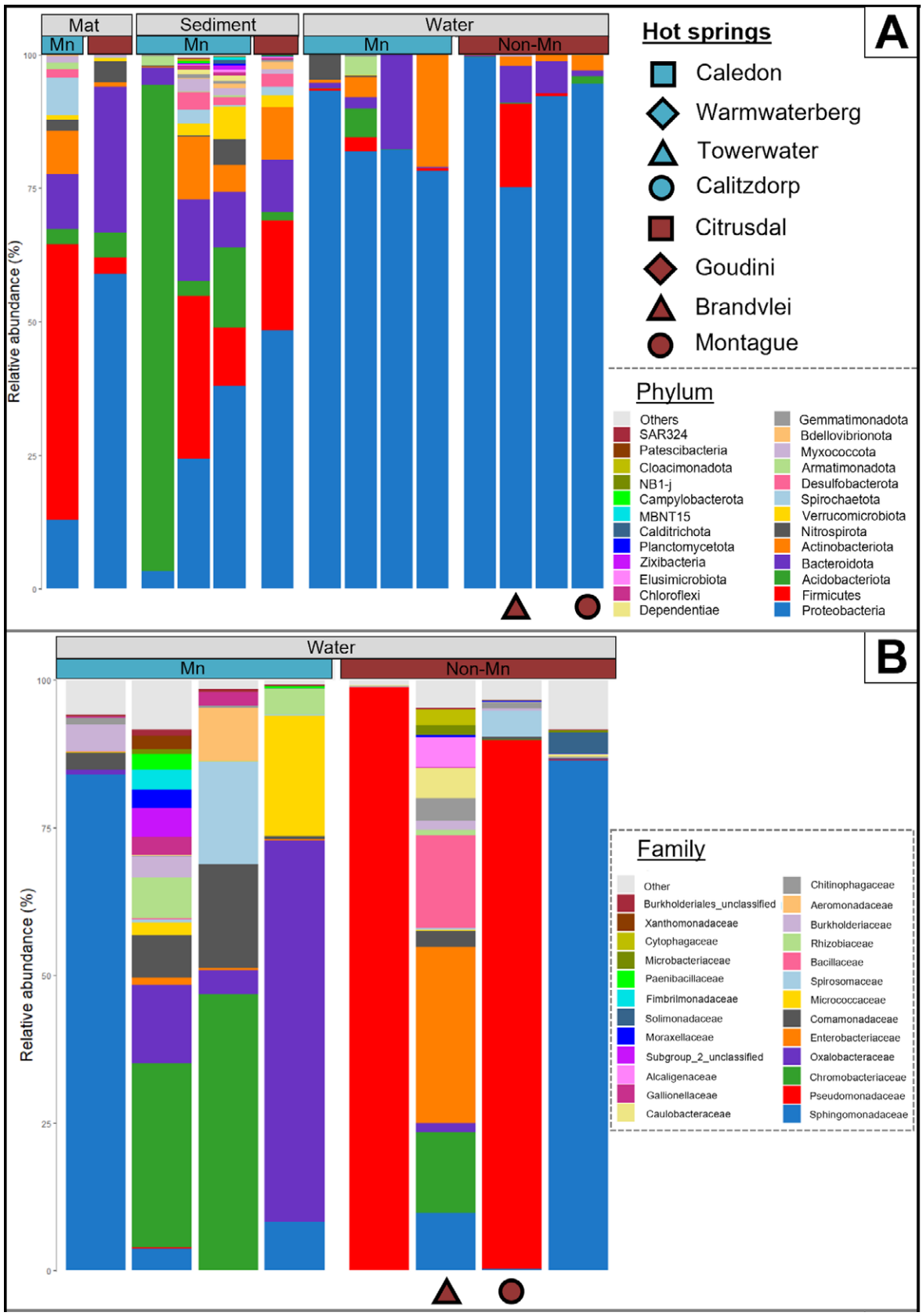

Figure 8 *(**A**) Microbiology test work results plotted according to the phylum abundance and diversity, normalised to 100%, for water, sediment and organic mat samples collected from each of the thermal spring study sites. (**B**) Family abundance and diversity plot, normalised to 100%, for water samples from the eight different study sites.*

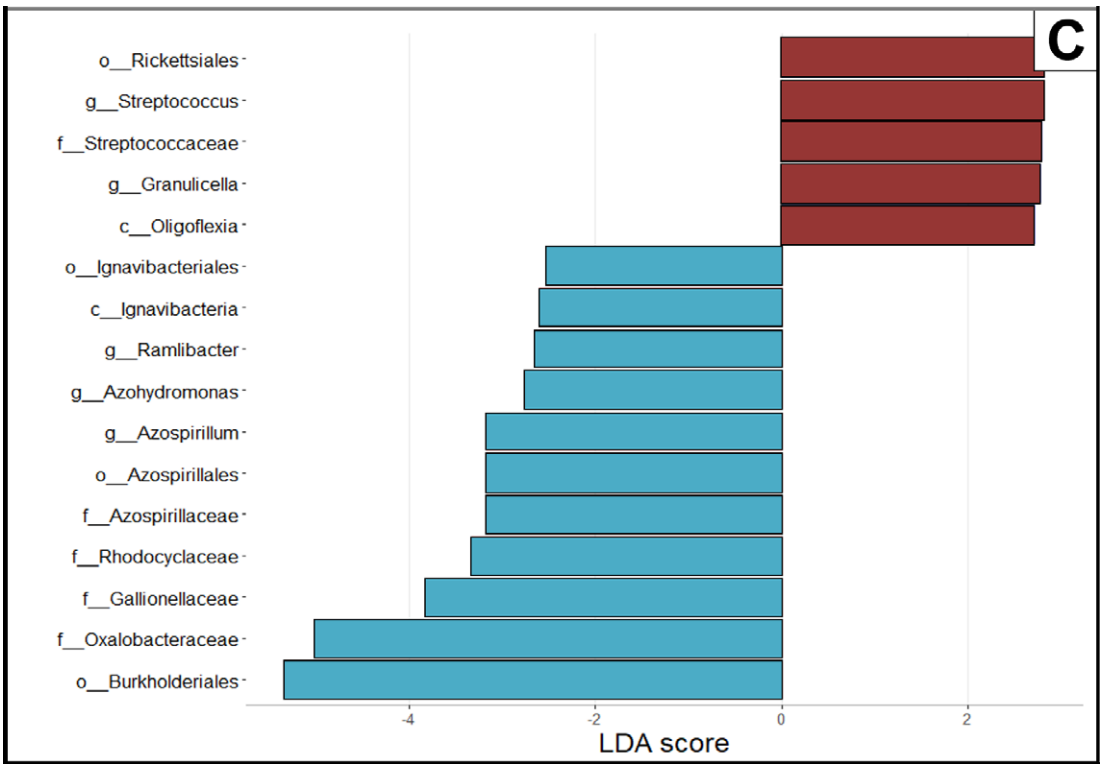

Figure 8 *(**C**) A Linear Discriminant Analysis diagram illustrating taxanomic units that display notable differences between the manganiferous and non-manganiferous spring water samples. Full microbiology DNA results are available in the Supplementary material. For enhanced image clarity, please consult the web version of the paper.*

an important control for the development of higher-grade occurrences (e.g. at Houtbay). As far as possible, our approach avoids these classification schemes and instead considers the formation of the various Mn occurrences from a process-oriented perspective (see next section). However, the sheer number of differences between the surficial mound-type Mn and the structurally-hosted Mn does qualify this broad classification. Indeed, from a process-oriented perspective, there is a fundamental difference between these two classes in that the surficial deposits are oxidised by having direct contact with atmospheric O_2, whereas the structurally-hosted deposits most likely form in a near-surface environment (e.g., McGregor, 2013; Killick, 2020) where the oxidising agent is likely a fluid phase (e.g., groundwater). Although Mn mounds and higher-temperature Mn sinters have received attention elsewhere globally (Hewett and Fleischer, 1960; Usui and Mita, 1995; Miura and Hariya, 1997), descriptions of the Cape mound-type Mn are rare in the scientific literature (Kent, 1949), whereas the structurally-hosted occurrences are much better documented. The present section offers a critical comparison between the two classes, highlighting commonalities and differences and offering a comment on the likelihood of a genetic linkage.

Outside of the obvious surficial vs. sub-surficial setting difference, the two classes of Mn occurrence display several notable textural, mineralogical and chemical differences. Given the absence of active water percolation into the structure-hosted deposits at the time of sampling, these deposits were not tested for the possible role of microbiology in the Mn mineralisation process. On a macroscale, the structure-hosted deposits typically show characteristics of open-space, in which well-formed crystalline Mn^{4+} oxides and oxyhydroxides prevail. Vein material typically has a glassy texture carrying a submetallic lustre (Figure 3). Adjacent to the primary vein networks, the Mn enrichment is much lower grade and commonly occupies interstitial loci between the discernable quartz grains of the host rock (generally sandstone). These low grade zones also commonly alternate and grade between being Fe-enriched versus Mn-enriched, and according to the relative proportions of these phases, carry colours that vary from orange/red/brown, through purple, to brown/black. Although this study focusses specifically on Mn, there is an intimate association between Fe and Mn at all the sites because of the similarities in the geochemical behaviour of the two third row transition metals. Most structure-hosted deposits show variable cross-cutting relationships between Fe-rich veins and Mn-rich veins, suggesting a complex temporal evolution of fracture opening and fluid infiltration. Decoupling of these two elements to achieve preferential concentration of Mn is achieved as a function of temperature gradients (typically in epithermal systems (e.g., Roy, 1988)), or as a function of the oxygen fugacity of the fluid (Mn is more easily reduced, i.e. at higher redox potential). In the Cape Mn occurrences, the latter process is likely to be more important, suggesting that more Mn-enriched occurrences form preferentially through the involvement of only slightly reducing groundwater conditions.

The mound-type deposits are more massive, yet highly friable, and predominantly have a dull lustre, except in discrete horizons where further upgrade has taken place by supergene/early diagenetic processes and associated mineral 'aging' mechanisms. These higher grade horizons were most clearly observed at the Caledon hot spring (Figures 2f, 3c and 3f), which was also the only mound-type deposit with quantifiable Mn^{4+} minerals (cryptomelane) using XRD. The bulk of the mineralogy of the mound comprises very small crystallite sizes (Figure 3f), and the general absence of notable XRD peaks, despite having elevated Mn concentrations (from XRF measurements (Table 2)), suggests that much of the Mn is hosted by poorly-crystalline and amorphous phases. Geochemically, the mound-type deposit class has higher average iron concentrations (51 ± 11 wt.%) relative to the structure-hosted deposits (19 ± 10 wt.%; Table 1).

In his evaluation of thermal springs around South Africa, Kent (1949) suggested that fracture-hosted Mn deposits in the greater Cape Town area may be related to extinct chalybeate and manganiferous thermal spring systems. From our results, it is not possible to unequivocally confirm or disprove this hypothesis, the testing of which can only truly be achieved by drilling into the fracture system below the sites of the currently-active manganiferous springs. Using a theoretical approach, a simple PhreeqC mixing model tested the interactions between a warm manganiferous spring fluid and cooler oxidising groundwater (Supplementary material). The model suggests that such an interaction results in a mixed fluid that is supersaturated with respect to e.g., haussmanite, pyrolusite, manganite and goethite. When modelling the interaction between warm non-manganiferous spring water and typical Cape ground water (Wu, 2008), the mixed fluid remains under-saturated with respect to manganite and hausmannite. Furthermore, the degree of supersaturation with respect to pyrolusite and goethite were respectively 74 to 77% and 17 to 27% less than in the model in which manganiferous spring water was used. Our tritium isotope results suggest that the sampled spring water has experienced very little mixing or dilution with ambient ground water (Figure 7). Although this may suggest that fluid mixing is not an important mechanism for Mn precipitation, it may also simply be an artefact of sampling the spring water that is being expelled at moderate to high flow rates and under positive pressure (Table 2; Diamond and Harris, 2000). That is, the main fluid mixing interface is peripheral to the main fluid flow pathway (Figure 9b).

There were two further observations that derived from our study of the mound-type Mn occurrences and which may have implications for the formation of the structurally-hosted sub-type. Firstly, at both the Warmwaterberg and the Towerwater sites, the current surficial water flow emanating from the springs (with corrected radiocarbon ages of ~15 000 years and 5 000 years respectively (Table 2 and Figure 7)) has clearly cut down through layers of earlier-formed Mn mound. This implies a period of uplift has occurred since the mounds started forming. The most recent geomorphic uplift event was the one at ~2.5 Ma that immediately preceded the Post-African II erosional cycle (Partridge and Maud, 1987). This potentially places a minimum

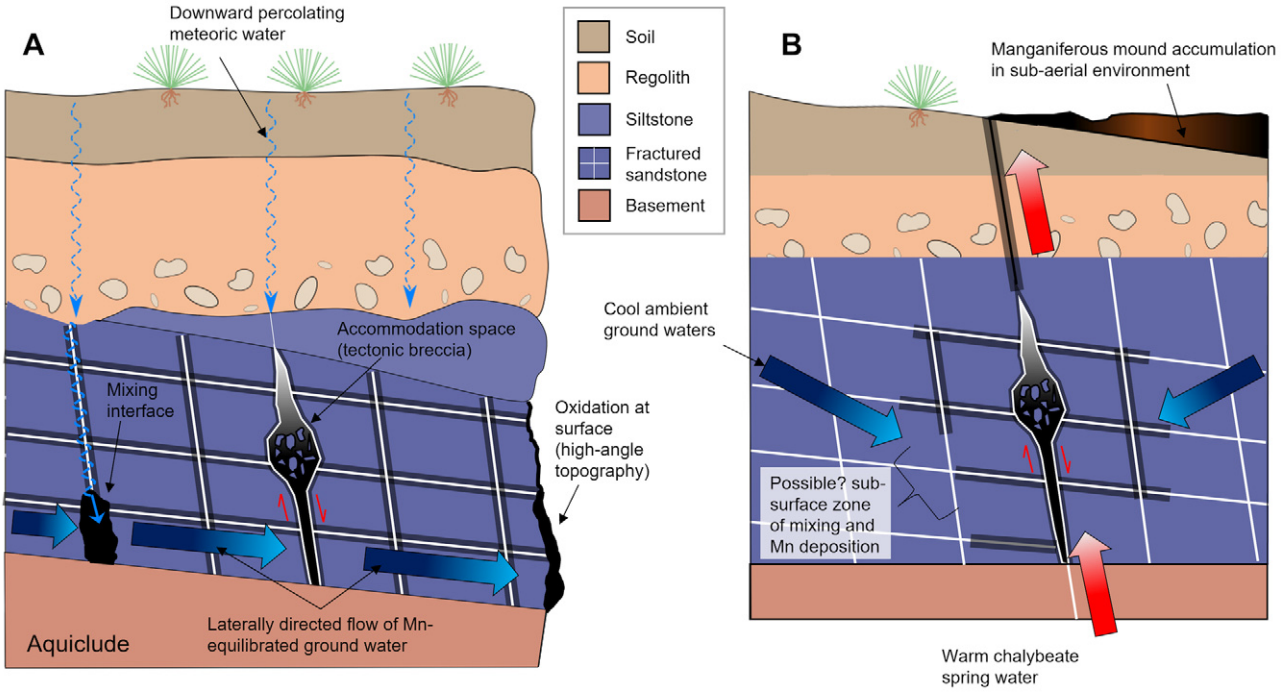

Figure 9 *(**A**) A model for the formation of the structure-hosted Mn deposits in which highly permeable sandstone units represent the preferred host rock, and focussed fluid flow and oxidising trap sites are needed to facilitate mineralisation (adapted from Compton, 2004). (**B**) A model illustrating the formation of sub-aerial Mn mound deposits directly related to the presence of chalybeate thermal springs. The existence of an associated subterranean Mn mineralising system remains tenuous. In both Mn deposit sub-classes, structural features such as faults represent crucial fluid flow pathways that enhance hydraulic permeability.*

age constraint on the longevity of the spring systems, which is somewhat older than a previous estimate of 850 000 years suggested by Kent (1947). This previous estimate was based on mass balance involving the mass of contained metal in the mounds, spring flow rates and spring water metal concentration. The longevity of these systems allows significant time for development of an associated subterranean system in e.g., second and third order structures or at a groundwater mixing interface (Figure 9b). The second implication derived from our work on the mounds was our observation of the ubiquity of Mn-oxidising microbial populations in the chalybeate spring waters and associated sediment and mat samples. Manganese-oxidising microbes have been implicated in the formation of ferromanganese nodules (Ehrlich, 2002; Southam and Saunders, 2005) and even in the world-class Kalahari Manganese Fields (Johnson et al., 2013). However, to the best of our knowledge, this highly-effectual mechanism for Mn precipitation has not previously been considered for the Cape's structure-hosted Mn occurrences, despite the known prevalence of the bioactive trace element phosphorus associated with these deposits.

Controls on metal concentration within the Cape Mn occurrences

Many of the Cape's Mn occurrences have been mined on a small scale historically (see Cole et al., 2014 and references therein), yet they are generally too phosphoric to serve as raw material for the steelmaking process. Depending on the Mn occurrence, decreased economic viability has also been attributed to factors such as small size, remote location, low grade, and the environmental sensitivity of the areas in which they are found (Kent, 1947; Cole et al., 2014). Accordingly, future mining of these deposits remains unlikely despite the emergence of technologies that remove P from Mn ores (Tu et al., 2019), and despite the niche uses of Mn^{4+}-rich minerals in the chemicals industry (e.g., in the oxidising agent potassium permanganate) and in reactive barriers (Li et al., 2021). Even though these are not Mn ores (*senso stricto*), a process-oriented approach (using the source-transport-trap model for understanding ore deposit formation) is useful towards understanding the Mn enrichments in both the mound- and structure-hosted occurrences. Importantly, the section lays out the multiple criteria that need to intersect to form a significant enrichment of Mn within the Cape's geology. Many of the sites evaluated did not fulfil all these criteria, thus explaining in part why they are sub-economic.

Source consideration 1- Source of metals: Early work conducted by Marchant et al. (1978) at the Houtbay deposit suggested that the arenites of the Cape Supergroup are six-fold enriched in Mn and three-fold enriched in Fe and P relative to world averages. Using mass balance and porosity arguments, McGregor (2013) corroborated this by also identifying the Peninsula Formation arenites as the source of Mn for several of the deposits in the Western Cape, although he stated that the more shale-rich Graafwater Formation may also be a viable source. Our analyses included the Bosjesmans Mn occurrence that is hosted in Malmesbury Group rocks (Figure 2b). This highlights that background Mn values are likely sufficiently high and sufficiently leachable in a range of sedimentary and metasedimentary lithologies in the greater Cape area.

Source considerations 2- Source of fluids: Existing literature contributions converge on a meteoric fluid source as the one that is most likely to give rise to the studied Mn occurrences. Magmatic sources are unlikely given that the last notable magmatic activity was the emplacement of the False Bay dyke swarm (~132 Ma (Reid et al., 1991)). Metamorphic fluids are ruled out because the Cape's geology is presently unroofing, and connate fluids are similarly excluded because expulsion of diagenetic fluids would have occurred >330 million years ago during burial stages of the Cape Supergroup (e.g., Thamm and Johnson, 2006). Our data for the various spring systems (Table 2), and the host of publications relating to the Cape aquifer (Diamond and Harris, 2000; Harris et al., 2010; Miller et al., 2017), confirm the efficacy of meteoric water recharge of the subterranean aquifer system.

Source considerations 3- Fluid characteristics: Based on mineral stability fields and understanding of Mn solubility, the slightly acidic rain- and ground-water characteristic of the Western Cape has a high affinity to solubilise Mn, especially once they become slightly reducing (e.g., Killick, 2020 and references therein). Our comparative study of the manganiferous and non-manganiferous spring waters highlights that several other factors may abet in enhancing Mn solubility and transport. The manganiferous spring water samples were characterised by having generally higher temperature, slightly higher pH and markedly higher salinity values relative to the non-manganiferous spring water samples (Figure 4 and Table 2). Although the pH control may be locally important through e.g., replacement of carbonate cement during sandstone replacement (Figure 3d), the salinity control is of particular importance as this is the ligand responsible for transporting Mn in geological fluids (Tian et al., 2014). The most manganiferous springs in our study, typically associated with Mn mound formation, had measured chloride concentration values ranging between 24 and 34 mg/l (Table 2), which is greater than the concentration measured in the non-manganiferous springs (11 and 18 mg/l).

Transport considerations 1- drivers of fluid flow: Using isotope data sets, Diamond and Harris (2000) have previously shown that spring systems in the Western Cape are recharged by meteoric fluid falling at relatively high altitude relative to the discharge site. Indeed, the mere fact that these springs are expelled under pressure (e.g., Brandvlei discharge rate = 126 l/s) implies the existence of a hydraulic head. Work by Dhansay and coworkers (2017) highlights the elevated geothermal gradient in the Cape Fold Belt, particularly in its syntaxis. Although this may aid in heating spring waters in accordance with the elevated geothermal gradient (>40°C/km; Dhansay et al., 2017), it is unlikely to be the major driver of fluid flow.

Transport considerations 2- fluid residence time: Our results present the first radiocarbon age data for many of these spring

water sampling sites. Importantly, Figure 7 highlights that the water samples from manganiferous springs are significantly older than those of the non-manganiferous springs. Since the residence time in an aquifer is a function of both the flow rate and the distance of the fluid pathway, the implications of a long residence time are two-fold. Firstly, if flow rate is the major control, then the increased time may result in greater opportunity for the fluid to reach its equilibrium Mn concentration (as defined by the Mn solubility limit). Secondly, if the length of the fluid pathway is the major control, then a longer flow path would increase the probability of the fluid interacting with horizons that have elevated Mn, and possibly Cl.

Transport considerations 3- rheology, permeability networks, aquicludes and fluid focusing: Figure 1 highlights that, with the exception of the Bosjemans site, all of the sampling sites fall within competent quartz arenites of the Peninsula Formation or the Rietvlei Formation (Nardouw Subgroup). Due to their competence, these units are particularly susceptible to brittle fracturing during deformation (i.e., during the Cape orogeny that gave rise to the Cape Fold Belt (280 to 260 Ma; Hansma et al., 2016)). Indeed, the associated fractured rock aquifer, known as the Table Mountain Group Aquifer, is recognised as being one of the largest and most important aquifer systems in South Africa (Miller et al., 2017). Although not all of the known Western Cape Mn occurrences were evaluated in this study (e.g. the several larger occurrences in Cedarberg region (de Villiers, 1960; Cole et al., 2014)), the prevalence of many noteworthy and evaluated structure-hosted sites and spring water sites in the syntaxis of Cape Fold Belt (Figure 1) may suggest a greater fracture density in this area. In contrast, impermeable units (e.g., basal silicified granite at Simonsberg; Malmesbury group rocks at Rooiels; Graafwater siltstone/shale at Houtbay (Figure 2)) serve to impede downward movement of meteoric fluids under gravity/hydraulic head and will instead direct the fluids laterally (Figure 9a). Manganese deposits ultimately form where this lateral flow intersects an oxidising front (i.e., the near surface and surface), commonly where the sub-horizontal strata and associated fluid flow are cut by high-angle relief of the ambient topography or by notable structures (e.g., faults and tectonic breccia zones).

Trapping considerations 1- local structures: All of the study sites were located in areas of some sort of structural complexity, typically in close proximity to large mapped faults. Similarly, the ultimate siting of the respective Mn occurrences was either within a notable structure (i.e., structurally-hosted sub-type) or at surface where spring waters are expelled from a structural conduit (i.e., Mn mound subtype). The importance of structures has been noted previously. For example, McGregor (2013) suggests that (cemented) faults represent zones of low effective porosity which may serve as barriers to continued down-dip groundwater flow and instead focus flow laterally in the adjacent fractured rocks. Long-lived structural features may have been preferentially exploited by prior dyke intrusions, opening up possibility for higher-grade Mn enrichments through replacement processes operating on the dyke saprolith (Killick, 2020). We suggest that the importance of the structures is two-fold. First, the more permeable faults/fracture zones may represent localised low points in the regional hydraulic gradient, into which fluid flow may actively focus. In instances where faults are still sporadically active (e.g., Worcester Fault (Bosjesmans), Colenso Fault (Simonsberg)), suction-pump type mechanisms may be of local importance and may explain some of the observed open-space filling textures (Figure 3e), and the successive episodes of coarser-grained Mn mineralisation (Figure 3g). Second, structures that extend to surface may hypothetically represent conduits for ingress of 'fresh' meteoric water. Where such localised oxidation fronts intersect with the 'equilibrated' laterally-migrating groundwaters, an efficient zone for Mn mineralisation may develop (Figure 9a).

Trapping considerations 2- precipitation mechanisms: Mineral stability fields are a function of many different physicochemical parameters including e.g., the oxygen fugacity, pH, temperature, salinity of the system. Given the general chemical inertness of quartz arenites, it is unlikely that wall-rock interactions are important for inducing Mn precipitation from the dissolved Mn (chloride) complexes. Given this inertness, a general absence of e.g., carbonate rocks which have the propensity to raise pH, and given that both ground and rain waters in the Cape are mildly acidic, previous authors have highlighted that pH increases are an unlikely mechanism to precipitate the observed Mn oxide minerals (e.g., Killick, 2020). Instead, an increase in the oxygen fugacity or Eh is suggested as the more probable mechanism. In the Mn mound deposits, this oxidation is easily achieved as the expelled spring waters can easily equilibrate with excess oxygen in the atmosphere. In the subterranean system, we suggest that oxidation is achieved preferentially in the near-surface environment where Mn-laden fluids may interact with oxidising groundwaters (Figure 9). The fluid-fluid interactions will additionally modify other parameters such as salinity and temperature, which impact Mn solubility, as shown in our modelled mixing experiments (Supplementary material). This near-surface criterion explains why several of the occurrences are known to pinch out at depth, and agrees with the observation of modern Mn cementing of recent talus slopes at e.g., Rooiels.

The role of manganese-oxidising microorganisms in precipitation of the Cape Mn occurrences has not previously been dealt with explicitly. Microorganisms that are capable of oxidising Mn^{2+} into insoluble Mn^{4+} oxides are known as Mn-oxidising microbes that can include eukaryotes and prokaryotes. In this study, we focused on determining the bacterial composition and distribution between manganiferous and non-manganiferous water samples, and determined which taxa were differentially represented. The phyla that were the most dominant in all samples included the Proteobacteria, Firmicutes, Acidobacteriota, Bacteroidota, and Actinobacteriota. These phyla have previously been identified as prevalent phyla in thermal spring samples (Cacciapuoti et al., 2020). No significant differences were observed in the community richness, evenness, or distribution between the manganiferous and non-manganiferous water samples. However, a few taxa were

identified that were differentially more abundant between these groups. In the manganiferous water samples, these included the orders Ignavibacteriales, Azospirillales, and Burkholderiales, families Azospirillaceae, Rhodocyclaceae, Gallionellaceae and Oxalobacteraceae, and genera *Ramlibacter*, *Azohydromonas*, and *Azospirillum*. Of these, the genus *Ramlibacter*, and members of Burkholderiales, Rhodocyclaceae, and Oxalobacteraceae, have been shown to oxidise manganese or contain genes for potential oxidation of manganese (Yu and Leadbetter, 2020; Cai et al., 2023; Sjöberg et al., 2020; Bushman et al., 2019). In most environments where manganese is abundant, it is commonly accepted that any bacteria found in these environments are capable of oxidising manganese. It is, however, important to note that some Mn-oxidisers are incapable of doing it alone and require the help from other functional microorganisms in the environment which could be represented in higher abundance. This could explain why a larger proportion of the population is represented by bacteria that are not known to oxidise manganese but could hold an important functional role in the spring environment.

Conclusion

By studying a diverse selection of structure-hosted Mn occurrences and mound-type Mn occurrences distributed throughout the Cape Fold Belt, we have built a more comprehensive and mechanistic understanding about how Mn enriches in the surface and near-surface environment. The two sub-classes of Mn occurrence are differentiated by their siting and by the medium responsible for Mn oxidation (i.e., contact with atmospheric O_2 at surface, fluid mixing with oxidising (and cooler) groundwaters in the subterranean environment). Although a direct linkage between the two remains equivocal until drilled, we posit that a non-reciprocal relationship exists. That is, it is possible that current thermal spring systems are underlain by a network of near-surface manganiferous veins (Figure 9b). However, not all hard-rock occurrences coincide with the loci of extinct thermal springs, and instead fluid may be focused towards a surficial oxidation front by an interplay between a gravity/hydraulic head and an impermeable lithological unit that is ultimately cut by the ambient topography. Irrespective of the focussing mechanism, factors that would enhance the probability of developing a significant deposit include involvement of an older, warmer, more saline, acidic and reducing fluid, a near-surface trap site with propensity for open space filling (possibly an active fault), and the presence of Mn-oxidising microbial communities. The mechanisms identified in the mound-type deposits, involving inorganic and biologically-mediated precipitation of fine crystallites that can subsequently age to coarser assemblages under early diagenetic conditions, may be more prevalent in other supergene Mn deposits globally. Linked to our microbiology investigation, the LDA analysis (Figure 8c) indicated many potential biomarkers that strongly associate with Mn, the strongest of which is that of Burkholderiales. Although it is unlikely that exploration will pursue blind Cape Mn targets, the documented biomarker signatures may find use as important fingerprinting tools.

Acknowledgements

The authors would like to thank the members of the CAF and iThema Laboratory who assisted with the various analytical investigations (M. Grobbelaar-Moolman (XRF); J. Colling (isotope geochemistry); R. Bucher (XRD)). We further thank Professor Alex Kisters for discussions, and the two reviewers (Professor John Compton and Professor Thierry De Putter) and the editorial staff Professor Marlina Elburg and Dr George Henry for the valuable comments that helped in strengthening the final submission. Financial support from DSI-NRF CIMERA and African Rainbow Minerals (BvdH) is also acknowledged and duly appreciated.

References

Andrews, J. and Kay, R., 1982. Natural production of tritium in permeable rocks. Nature 298, 361-363. doi:10.1038/298361a0

Astrup, J. and Tsikos, H., 1998. Manganese. In: M.G.C. Wilson and C.R. Anhaeusser (Editors), The Mineral Resources of South Africa, Council for Geoscience, Pretoria, South Africa, 450-460.

Baker, A.A., Duncan, D.C. and Hunt, C.B., 1952. Manganese deposits of southeastern Utah. Geological Survey Bulletin No. 979-B. United States Government Publishing Office.

Beukes, N.J., Swindell, E.P. and Wabo, H., 2016. Manganese deposits of Africa. Episodes Journal of International Geoscience, 39, 285-317.

Blewett, S.C., Phillips, D. and Matchan, E.L., 2019. Provenance of Cape Supergroup sediments and timing of Cape Fold Belt orogenesis: Constraints from high-precision $^{40}Ar/^{39}Ar$ dating of muscovite. Gondwana Research, 70, 201-221.

Bushman, T.J., Akob, D.M., Bohu, T., Beyer, A., Woyke, T., Shapiro, N., Lapidus, A., Klenk, H.P. and Küsel, K., 2019. Draft genome sequence of Mn (II)-oxidizing bacterium Oxalobacteraceae sp. Strain AB_14. Microbiology Resource Announcements, 8, 10-1128.

Cacciapuoti, S., Luciano, M.A., Megna, M., Annunziata, M.C., Napolitano, M., Patruno, C., Scala, E., Colicchio, R., Pagliuca, C., Salvatore, P. and Fabbrocini, G., 2020. The role of thermal water in chronic skin diseases management: a review of the literature. Journal of Clinical Medicine, 9, 3047.

Cai, Y., Yang, K., Qiu, C., Bi, Y., Tian, B. and Bi, X., 2023. A Review of Manganese-Oxidizing Bacteria (MnOB): Applications, Future Concerns, and Challenges. International Journal of Environmental Research and Public Health, 20, 1272.

Carmichael, S.K., Doctor, D.H., Wilson, C.G., Feierstein, J. and McAleer, R.J., 2017. New insight into the origin of manganese oxide ore deposits in the Appalachian Valley and Ridge of northeastern Tennessee and northern Virginia, USA. Geological Society of America Bulletin, 129, 1158-1180.

Chan, M.A., Parry, W.T. and Bowman, J.R., 2000. Diagenetic hematite and manganese oxides and fault-related fluid flow in Jurassic sandstones, southeastern Utah. American Association of Petroleum Geologists Bulletin, 84, 1281-1310.

Cole, D.I., Ngcofe, L. and Halenyane, K., 2014. Mineral commodities in the Western Cape Province, South Africa. Council for Geoscience, Western Cape Regional Office, Report, 12, 90pp

Compton, J.S., 2004. The rocks and mountains of Cape Town. Double Story Books. 112pp

Conradie, T.A. and Jacobs, K., 2021. Distribution patterns of Acidobacteriota in different fynbos soils. PLoS ONE, 16, e0248913.

Dhansay, T., Musekiwa, C., Ntholi, T., Chevallier, L., Cole, D. and de Wit, M.J., 2017. South Africa's geothermal energy hotspots inferred from subsurface temperature and geology. South African Journal of Science, 113, 1-7.

De Villiers, J., 1960. The manganese deposits of the Union of South Africa: Geological Survey of South Africa, Pretoria, Handbook 2, 280pp

Diamond, R.E. and Harris, C., 2000. Oxygen and hydrogen isotope geochemistry of thermal springs of the Western Cape, South Africa:

recharge at high altitude? Journal of African Earth Sciences, 31, 467-481.

Edgar, R.C., Haas, B.J., Clemente, J.C., Quince, C. and Knight, R., 2011. UCHIME improves sensitivity and speed of chimera detection. Bioinformatics, 27, 2194-2200.

Ehrlich, H.L., 2002. Geomicrobiology, 4th ed.: New York, Marcel Dekker. 800pp

Eriksson, P.G., Reczko, B.F.F. and Callaghan, C.C., 1997. The economic mineral potential of the mid-Proterozoic Waterberg Group, northwestern Kaapvaal craton, South Africa. Mineralium Deposita, 32, 401-409.

Fisher, R.A., Corbet, A.S. and Williams, C.B., 1943. The relation between the number of species and the number of individuals in a random sample of an animal population. Journal of Animal Ecology, 12, 42. doi:10.2307/1411

Flint, S.A., Hodgson, D.M., Sprague, A.R., Brunt, R.L., van der Merwe, W.C., Figueiredo, J., Prélat, A., Box, D., Di Celma, C. and Kavanagh, J.P., 2011. Depositional architecture and sequence stratigraphy of the Karoo basin floor to shelf edge succession, Laingsburg depocentre, South Africa. Marine and Petroleum Geology, 28, 658-674.

Gresse, P.G. and Theron, J.N., 1992. The geology of the Worcester area, Explanation Sheet 3319. Geological Survey of South Africa, Pretoria, 79pp

Hansma, J., Tohver, E., Schrank, C., Jourdan, F. and Adams, D., 2016. The timing of the Cape Orogeny: New $^{40}Ar/^{39}Ar$ age constraints on deformation and cooling of the Cape Fold Belt, South Africa. Gondwana Research, 32, 122-137.

Harris, C., 2023. O-and H-isotope record of Cape Town rainfall from 1996 to 2022: the effect of increasing temperature, and the 'water crisis' of 2015 to 2018. South African Journal of Geology, 126, 515-528.

Harris, C., Burgers, C., Miller, J. and Rawoot, F., 2010. O-and H-isotope record of Cape Town rainfall from 1996 to 2008, and its application to recharge studies of Table Mountain groundwater, South Africa. South African Journal of Geology, 113, 33-56.

Hewett, D.F. and Fleischer, M., 1960. Deposits of the manganese oxides. Economic Geology, 55, 1-55.

Johnson, J.E., Webb, S.M., Thomas, K., Ono, S., Kirschvink, J.L. and Fischer, W.W., 2013. Manganese-oxidizing photosynthesis before the rise of cyanobacteria. Proceedings of the National Academy of Sciences 110, 11238-11243.

Jones, T.V., 2010. Old Cape Town Mines. Cape Town Gem & Mineral Club website, viewed 21 January 2024. http://ctminsoc.org.za/articles/old-cape-town-mines

Kent, L.E., 1949. The thermal waters of the Union of South Africa and South West Africa. Transactions of the Geological Society of South Africa, 52, 231-264.

Killick, A.M., 2020. The setting and style of manganese mineralization in the Constantiaberg Massif, Cape Peninsula, South Africa. South African Journal of Geology, 123, 493-510.

Kisters, A.F., Belcher, R.W., Scheepers, R., Rozendaal, A., Jordaan, L.S. and Armstrong, R.A., 2002. Timing and kinematics of the Colenso Fault: The Early Paleozoic shift from collisional to extensional tectonics in the Pan-African Saldania Belt, South Africa. South African Journal of Geology, 105, 257-270.

Laznicka, P., 1992. Manganese deposits in the global lithogenetic system: Quantitative approach. Ore Geology Reviews, 7, 279-356.

Li, Y., Huang, Y., Wu, W., Yan, M. and Xie, Y., 2021. Research and application of arsenic-contaminated groundwater remediation by manganese ore permeable reactive barrier. Environmental Technology, 42, 2009-2020.

Liu, C., Cui, Y., Li, X. and Yao, M., 2021. Microeco: an R package for data mining in microbial community ecology. Federation of European Microbiological Societies, Microbiology Ecology, 97, fiaa255, 9pp. doi: 10.1093/femsec/fiaa255

MacGregor, D.G., 2013. Manganese deposits of the Cape Peninsula, South Africa. Unpublished MSc thesis, University of Cape Town, South Africa, 139pp

Marchant, J.W., Willis, J.P. and Duncan, A.R., 1978. Geochemistry of the Table Mountain Group, 1: Aspects of the origin of the Houtbaai manganese deposit. Transactions of the Geological Society of South Africa, 81, 179-184.

McCuaig, T.C., Beresford, S. and Hronsky, J., 2010. Translating the mineral systems approach into an effective exploration targeting system. Ore Geology Reviews, 38, 128-138.

Miller, J.A., Dunford, A.J., Swana, K.A., Palcsu, L., Butler, M. and Clarke, C.E., 2017. Stable isotope and noble gas constraints on the source and residence time of spring water from the Table Mountain Group Aquifer, Paarl, South Africa and implications for large scale abstraction. Journal of Hydrology, 551, 100-115.

Miura, H. and Hariya, Y., 1997. Recent manganese oxide deposits in Hokkaido, Japan. Geological Society, London, Special Publications, 119, 281-299.

Palcsu, L., Major, Z., Köllő, Z. and Papp, L., 2010. Using an ultrapure ^{4}He spike in tritium measurements of environmental water samples by the ^{3}He-ingrowth method. Rapid Communications in Mass Spectrometry, 24, 698-704.

Partridge, T.C. and Maud R.R., 1987. Geomorphic evolution of southern Africa since the Mesozoic. South African Journal of Geology, 90, 179-208.

Reid, D.L., Erlank, A.J. and Rex, D.C., 1991. Age and correlation of the False Bay dolerite dyke swarm, south-western Cape, Cape Province. South African Journal of Geology, 94, 155-158.

Roy, S., 1968. Mineralogy of the different genetic types of manganese deposits. Economic Geology, 63, 760-786.

Roy, S., 1997. Genetic diversity of manganese deposition in the terrestrial geological record. Geological Society, London, Special Publications, 119, 5-27.

Schloss, P.D., Westcott, S.L., Ryabin, T., Hall, J.R., Hartmann, M., Hollister, E.B., Lesniewski, R.A., Oakley, B.B., Parks, D.H., Robinson, C.J. and Sahl, J.W., 2009. Introducing mothur: open-source, platform-independent, community-supported software for describing and comparing microbial communities. Applied and Environmental Microbiology, 75, 7537-7541.

Shannon, C.E., 1948. A mathematical theory of communication. The Bell System Technical Journal, 27, 379-423. doi:10.1002/j.1538-7305.1948.tb01338.x

Simpson, E.H., 1949. Measurement of diversity. Nature, 163, 688. doi:10.1038/163688a0

Sjöberg, S., Stairs, C.W., Allard, B., Homa, F., Martin, T., Sjöberg, V., Ettema, T.J. and Dupraz, C., 2020. Microbiomes in a manganese oxide producing ecosystem in the Ytterby mine, Sweden: impact on metal mobility. Federation of European Microbiological Societies, Microbiology Ecology, 96, fiaa169, 17pp https://doi.org/10.1093/femsec/fiaa169

Southam, G. and Saunders, J.A., 2005. The geomicrobiology of ore deposits. Economic Geology, 100, 1067-1084.

Steenkamp, J.D., Chetty, D., Singh, A., Hockaday, S.A.C. and Denton, G.M., 2020. From ore body to high temperature processing of complex ores: manganese – a South African perspective. The Journal of The Minerals, Metals & Materials Society, 72, 3422-3435.

Thamm, A.G. and Johnson, M.R., 2006. The Cape Supergroup. In: M.R. Johnson, C.R. Anhaeusser, and R.J. Thomas (Editors), The Geology of South Africa. Geological Society of South Africa, Johannesburg/Council for Geoscience, Pretoria, 443-460.

Theron, J.N., 1984. The geology of Cape Town and environs. Explanation of Sheets 3318 CD and DC, and 3418 AB and BA (Scale 1:50000). Geological Survey of South Africa, Pretoria, 77pp

Tian, Y., Etschmann, B., Mei, Y., Grundler, P.V., Testemale, D., Hazemann, J., Elliott, P. and Ngothai, Y., 2014. Speciation and thermodynamic properties of manganese(II) chloride complexes in hydrothermal fluids: *in situ* XAS study. Geochimica et Cosmochimica Acta, 129, 77-95. doi:10.1016/j.gca.2013.12.003

Nicholson, K., 1988. An ancient manganese-iron deposit of freshwater origin, Islay, Argyllshire. Scottish Journal of Geology, 24, 175-187.

Nicholson, K., 1989. Manganese minerals in Scotland. Scottish Journal of Geology, 25, 125-142.

Tu, Z., Liang, X., Wang, Y. and Wu, C., 2019. Removal of phosphorus from high-phosphorus manganese ores by ammonia-ammonium carbonate leaching method. Metals, 9, 1354.

United States Geological Survey, 2023. Manganese Statistics and Information, 2023 Edition. https://pubs.usgs.gov/periodicals/mcs2023/mcs2023-manganese.pdf

Usui, A. and Mita, N., 1995. Geochemistry and mineralogy of a modern

buserite deposit from a hot spring in Hokkaido, Japan. Clays and Clay Minerals, 43, 116-127.

Van Rooyen, J.D., Palcsu, L., Visser, A., Vennemann, T.W. and Miller, J.A., 2021. Spatial and temporal variability of tritium in precipitation within South Africa and it's bearing on hydrological studies. Journal of Environmental Radioactivity, 226, 106354.

Van Rooyen, J.D., Watson, A.W. and Miller, J.A., 2022. Using tritium and radiocarbon activities to constrain regional modern and fossil groundwater mixing in Southern Africa. Journal of Hydrology, 614, 128570.

Welsh, A.B., 1917. Report on the manganese deposits in the South-West Districts of the Cape Province, Union of South Africa, Cape Times Limited, Government Printers. U.G.34-17.

Wu, C., 2008. Groundwater occurrence in the Table Mountain area of Cape Town, South Africa. M.Sc. Thesis, University of the Western Cape, South Africa. 124pp

Yu, H. and Leadbetter, J.R., 2020. Bacterial chemolithoautotrophy via manganese oxidation. Nature, 583, 453-458.

Editorial handling: M.A. Elburg.